J. Fluid Mech. (1991), *vol.* 223, *pp.* 631–661
Printed in Great Britain

Buoyant inhibition of Ekman transport on a slope and its effect on stratified spin-up

By PARKER MACCREADY AND PETER B. RHINES
School of Oceanography, WB-10, University of Washington, Seattle, WA 98195 USA

(Received 5 September 1989 and in revised form 3 August 1990)

The unsteady boundary layer of a rotating, stratified, viscous, and diffusive flow along an insulating slope is investigated using theory, numerical simulation, and laboratory experiment. Previous work in this field has focused either on steady flow, or flow over a conducting boundary, both of which yield Ekman-type solutions. After the onset of a circulation directed along constant-depth contours, Ekman-type flux up or down the slope is opposed by buoyancy forces. In the unsteady, insulating case, it is found that the cross-slope transport decreases in time as $(t/\tau)^{-\frac{1}{2}}$ where

$$\tau = \frac{1}{S^2 f \cos\alpha}\left(\frac{1/\sigma + S}{1+S}\right),$$

may be called the 'shut-down' time. Here $S = (N\sin\alpha/f\cos\alpha)^2$, f is the Coriolis frequency, α is the slope angle, N is the buoyancy frequency, and σ is the Prandtl number. Subsequently the along-slope flow, $\hat{v}$, approximately obeys a simple diffusion equation

$$\frac{\partial \hat{v}}{\partial t} = \nu\left(\frac{1/\sigma + S}{1+S}\right)\frac{\partial^2 \hat{v}}{\partial \hat{z}^2},$$

where t is time, ν is the kinematic viscosity, and $\hat{z}$ is the coordinate normal to the slope. By this process the boundary layer diffuses into the interior, unlike an Ekman layer, but at a rate that may be much slower than would occur with simple non-rotating momentum diffusion. The along-slope flow, $\hat{v}$, is nevertheless close to thermal wind balance, and the much-reduced cross-slope transport is balanced by stress on the boundary. For a slope of infinite extent the steady asymptotic state is the diffusively driven 'boundary-mixing' circulation of Thorpe (1987). By inhibiting the cross-slope transport, buoyancy virtually eliminated the boundary stress and hence the 'fast' spin-up of classical theory in laboratory experiments with a bowl-shaped container of stratified, rotating fluid.

1. Introduction

1.1. *Ekman layer on a slope with stratification*

The Ekman layer has a cross-isobar transport (the 'Ekman transport'), which, if horizontally divergent, drives a vertical velocity out of the boundary layer. This vertical velocity stretches or shrinks vortex lines in the interior, and the boundary layer may thereby affect large-scale atmospheric or oceanic flows, a process called 'spin-up'. The review article by Benton & Clark (1974) gives the early history of spin-up in many different contexts. If the fluid is stratified and the boundary is sloping, then buoyancy forces may impede the Ekman transport, lessening the vertical velocity, and significantly decreasing the effect of the boundary on the interior. In

this paper we derive a theory of the boundary layer for rotating, stratified flow along a slope and then compare this theory with numerical and laboratory experiments.

Several authors have considered the flow of a rotating, stratified, viscous fluid over topography. By 'topography' we mean any boundary whose normal is not parallel to gravity. Fluid over such terrain may have isopycnals intersecting the slope, and hence there will be gradients of density on the slope. Above a flat boundary, scaling arguments (Pedlosky 1987, pp. 360–362) suggest that, if buoyancy and Coriolis forces are comparable in a depth H (the vertical scale of the interior flow), then buoyancy may be negligible within a boundary layer much thinner than H. This argument is often used (e.g. Pedlosky 1987, equation 6.6.9) to justify the use of simple Ekman theory for oceans or atmospheres with sloping lower boundaries. With a sloping boundary, however, persistent advection of buoyancy contrasts may eventually introduce significant new effects. The key effect is the excursion of fluid particles within the boundary layer, which tends to be far larger than that in the interior. During spin-up, for example, the classic solution without stratification shows excursion of near-boundary fluid through a distance $L(\epsilon H/\delta)$, which may readily exceed L, the lateral scale of the flow. Here δ is the thickness of the Ekman layer, $(\nu/\Omega)^{\frac{1}{2}}$, where ν is the kinematic viscosity, and Ω is the rotation rate of the fluid. The Rossby number, ϵ, is $U/\Omega L$, where U is the scale of the horizontal velocity. Although ϵ is typically small for large-scale geophysical flows, H/δ is typically large.

Holton (1967) first solved for a 'buoyant' Ekman layer when studying atmospheric flow over the Great Plains of the United States, a region of gradually sloping terrain. The density in Holton's model boundary layer has diurnal radiative forcing, with a specified temperature (and hence density) at the ground. An along-slope, geostrophic wind is specified in the interior. He finds that the boundary layer is a modified Ekman spiral, plus a thermally driven diurnal oscillation. The effect of the slope combined with the stratification is to create a buoyancy force which decreases the magnitude of the diurnal oscillation. Yet there is also a steady cross-slope transport associated with the mean along-slope wind. This steady transport is possible because, for example, as the Ekman transport drives cold, heavy air up-slope, this air is warmed by internal diabatic heating, forced by the temperature boundary condition.

Hsueh (1969) also solved for a buoyant Ekman layer, again specifying the flow in the interior and the temperature at the boundary. His analysis is for shallow slopes ($\alpha \ll 1$, where α is the slope angle from horizontal) and allows horizontal variation of the slope. His solution is similar to an Ekman layer, but of reduced thickness: $\delta(1+\sigma(\alpha N/f)^2)^{-\frac{1}{4}}$, where σ is the Prandtl number, ν/κ, and κ is the density diffusivity. N is the buoyancy frequency, and f is the Coriolis frequency, 2Ω. As in Holton's solution a steady up-slope transport is allowed by the diffusion of heat to or from the boundary.

If the sloping boundary is insulating instead of conducting, the buoyancy can no longer adjust as fluid moves up- or down-slope, except in the presence of diffusion to the interior. The cross-slope buoyancy flux must nevertheless enter into the force balance. Siegmann (1971), considering stratified spin-up in a spherical container with conducting walls, suggests that if the walls are insulating rather than conducting then there may be no order-one fast spin-up, since cross-slope boundary layer transport will be suppressed by the buoyancy. Our laboratory experiments (§5) show this to be largely correct in the limit of strong stratification and steep walls, but even in this limit there were unexpected results. For example, we found that the boundary layer was no longer confined to the narrow Ekman layer thickness, but instead diffused far into the interior.

Weatherly & Martin (1978) developed a numerical model of the turbulent boundary layer along a sloping ocean bottom, comparing it with data from the Western Atlantic on the continental slope. They account for buoyancy forces in their calculation, and one may observe in their model results (see their figure 9) a gradual slowing of the up-slope Ekman transport, although the calculation is not carried very far in time.

Above an insulating slope, such as the ocean floor, the boundary conditions for temperature and salinity require that isopycnal surfaces lie normal to the boundary. This is accomplished by diffusion, but the resulting tilted isopycnals are not in balance with buoyancy forces. For a non-rotating fluid the result, Phillips (1970), is a steady up-slope boundary layer current wherein up-slope advection of the density gradient exactly balances the diffusive down-slope density flux. Oceanographic attention has been focused recently on this class of 'self-propelled' boundary-layer flows (Phillips, Shyu & Salmun 1986; Thorpe 1987, and Garrett 1990) because of the possibility that enhanced mixing occurs at ocean boundaries. Diffusively driven flows on sloping boundaries may both mix stratified fluid and exchange fluid with the interior.

Thorpe (1987) discussed the boundary layer of a rotating, stratified, viscous, diffusive flow along an insulating slope of constant angle and infinite extent. His solution plays an important role in the time-dependent model developed below in §2. It is steady, with a vertical structure much like Hsueh's (1969) solution. Yet on application of the insulating boundary condition Thorpe finds that the interior flow far from the boundary is specified as a part of the solution. Thus, while steady solutions exist for any interior flow if density is specified at the boundary (as we see in Holton 1967 and Hsueh 1969), there is only one interior flow that has a steady boundary layer in the insulating case. Thorpe, like Holton, also presents an oscillatory solution, but it must oscillate about the steady solution, and the time-averaged properties are unchanged. For uniform ν and κ, the steady flow in Thorpe's solution is one that leads to an up-slope transport. This up-slope flow is allowed because it is balanced by a diffusive down-slope density flux, driven by the density boundary condition, as in the non-rotating solution of Phillips (1970). The boundary layer is, like the Ekman layer, confined to a thin region, and is unable to alter the interior except through meridional circulation.

The diversity of steady solutions in the literature, corresponding to different boundary conditions and values of σ, suggests the need for a theory with more than oscillatory time-dependence. What happens, for example, when an interior along-slope flow is 'switched-on' to a value different than Thorpe's? At one extreme (early time) the problem yields Ekman theory, in which the interior flow controls the boundary layer, which then feeds back on the interior by Ekman pumping. At the other extreme (late time) lies Thorpe's solution, where a steady boundary layer requires a particular value of the interior velocity, although how this state comes about is unclear. In more general applications, the presence of other insulating boundaries will cause the fluid eventually to be well-mixed and at rest, in the absence of sources or sinks of momentum or buoyancy. This suggests that it is crucial to know the rate of establishment of the quasi-steady Ekman- and boundary-mixing solutions, for they must compete with the external forcing affects that maintain the circulation and stratification of the fluid. We can anticipate a strong dependence on σ, and in particular a weakness of the boundary-mixing circulations for the large values of σ typical of laminar conditions in laboratory experiments.

1.2. *Classic spin-up*

While the boundary layer is accessible to theory and numerical solution, its small size makes visualization difficult in laboratory experiments. But we may readily observe the large-scale effects of boundary-layer transport in spin-up experiments. In the classic spin-up problem (Greenspan & Howard 1963) a right circular cylinder filled with homogenous, incompressible, viscous fluid is rotating initially at angular velocity Ω. The cylinder is then impulsively accelerated to a slightly greater angular velocity $\Omega+\Delta\Omega$. In a time $O(\Omega^{-1})$ an Ekman layer forms on the bottom boundary (we take the top to be a free surface). The ensuing Ekman transport drives a meridional circulation involving radial and vertical velocities in the interior. The interior fluid never directly feels the effects of viscosity, and approaches the new rotation rate in a timescale $E^{-\frac{1}{2}}\Omega^{-1}$, where E is the Ekman number, $(\delta/H)^2$, and H is the height of the cylinder. For small Ekman number this spin-up timescale is much faster than that for penetration of viscous effects into the interior, $E^{-1}\Omega^{-1}$. For typical laboratory parameters ($\nu = 0.01$ cm^2 s^{-1}, $\Omega = 1$ s^{-1}, $H = 10$ cm) the 'fast' spin-up occurs in 100 s, whereas the viscous timescale is nearly three hours, and this contrast is magnified in flows of geophysical scale.

It is essential to incorporate stratification if spin-up is to apply to atmosphere and ocean flows. Holton (1965) divides the equations of motion into interior and boundary-layer parts, scaling vertical derivatives in the boundary layer as $E^{-\frac{1}{2}}$ greater than those in the interior. He takes the timescale of the problem to be the 'fast' spin-up time, $E^{-\frac{1}{2}}\Omega^{-1}$, based on the results of Greenspan & Howard (1963), and expands all dependent variables in powers of $E^{\frac{1}{2}}$, the obvious small parameter of the problem.

The primary result of Holton's analysis is that the 'fast' spin-up process no longer extends through the entire depth of the fluid, but is confined by the buoyancy within a 'Prandtl scale' $H_{\mathrm{P}} = fL/N$ above the bottom boundary (the subscript P is for Prandtl). L is the horizontal lengthscale of the forcing, typically the tank radius. Holton also finds that stratified spin-up is faster than in the homogenous case, owing to the reduced height of penetration, H_{P}. At the end of the 'fast' spin-up process the fluid in the interior has considerable vertical shear, which is removed by viscosity. Diffusive effects at $O(E^{\frac{1}{2}})$ and $O(E)$ were considered by St-Maurice & Veronis (1975), who find both a gradual migration to a diffusively controlled interior, and modification of the 'fast' spin-up by viscosity.

Spin-up theory has provided justification for a simple parameterization of bottom boundary friction of geophysical flows, essentially as a surface drag that is linear in the geostrophic velocity. Numerical and analytical models of large-scale flow thus often assume that relative vorticity decays exponentially with timescale $E^{-\frac{1}{2}}\Omega^{-1}$, rather than resolve the boundary layer itself. The exact timescale is, in practice, difficult to determine because δ and H_{P} are hard to measure, but their variation is not so great as to make the theory unworkable.

In §2 we develop the boundary-layer equations, and derive approximate time-dependent solutions for an insulating boundary with constant ν and κ, and an impulsively started interior flow. We compare these to numerical solutions to the full one-dimensional problem in §3. The balance of the paper is a description and discussion of laboratory experiments. We carried out stratified spin-up experiments in a container with a sloping bottom boundary, using stratification large enough to inhibit Ekman transport well before 'fast' spin-up could influence the interior flow.

2. The time-dependent Ekman layer with stratification

2.1. *Development of the equations*

The equations of motion and mass conservation for a Boussinesq, incompressible fluid, in a reference frame rotating at angular velocity $\Omega \boldsymbol{k}$ may be written as

$$\frac{\mathrm{d}\boldsymbol{u}}{\mathrm{d}t}+f(\boldsymbol{k}\times\boldsymbol{u})=-\frac{\nabla p}{\rho_0}-\frac{g\rho\boldsymbol{k}}{\rho_0}+\nu\nabla^2\boldsymbol{u}, \tag{2.1a}$$

$$\frac{\mathrm{d}\rho}{\mathrm{d}t}=\kappa\nabla^2\rho, \tag{2.1b}$$

$$\nabla\cdot\boldsymbol{u}=0. \tag{2.1c}$$

Here $\boldsymbol{u}$ is the velocity vector (u,v,w) in Cartesian coordinates (x,y,z), ∇ is the gradient $(\partial/\partial x, \partial/\partial y, \partial/\partial z)$, $\mathrm{d}/\mathrm{d}t$ is the material derivative $\partial/\partial t+\boldsymbol{u}\cdot\nabla$, $\boldsymbol{k}$ is the vertical unit vector $(0,0,1)$, and g is gravity.

The density ρ has been separated into three parts such that

$$\rho=\rho_0+\overline{\rho}(z)+\rho'(x,y,z,t). \tag{2.2}$$

We wish to consider a system with small density variations from the mean, ρ_0, hence $\rho' \ll \rho_0$ and $\overline{\rho} \ll \rho_0$. We allow ρ' to be as large as $\overline{\rho}$, so that the time-dependent density variation could, for example, overwhelm the static stability of the stratification. We define the buoyancy frequency by

$$N^2=-\frac{g}{\rho_0}\frac{\partial\overline{\rho}}{\partial z}. \tag{2.3}$$

We take N to be constant in our analysis.

The pressure p is separated into two parts:

$$p=\overline{p}(x,z)+p'(x,y,z,t). \tag{2.4}$$

The z-dependence of $\overline{p}$ is taken to be hydrostatic, hence

$$\frac{\partial\overline{p}}{\partial z}=-g(\rho_0+\overline{\rho}). \tag{2.5}$$

The x-dependence of $\overline{p}$ is used to introduce an along-slope geostrophic velocity, V, in the interior, given by

$$V=\frac{1}{f\rho_0}\frac{\partial\overline{p}}{\partial x}. \tag{2.6}$$

V is constant in both time and space (after time $t=0$), and is specified as an initial condition of the problem.

We want to describe the development of the boundary layer for flow along a slope. Following Phillips (1970) we simplify the problem by considering flow along a boundary of constant slope, $\tan\alpha$. While this one-dimensional geometry also eliminates boundary-layer divergence, parametric variations of interior velocity or slope can later incorporate this 'pumping', which is crucial to classic spin-up. We then rotate the equations into the slope frame of reference, as defined in figure 5(*b*). All variables in the new frame of reference will be denoted by $\hat{}$. The rotated velocity vector components are the up-slope velocity $\hat{u}$, the along-slope velocity $\hat{v}$, and the velocity normal to the slope, $\hat{w}$, in the corresponding Cartesian coordinate system, $\hat{x}$,

$\hat{y}$, $\hat{z}$. We assume $\hat{u}$, $\hat{v}$, $\hat{w}$, ρ', and p' have no $\hat{x}$ or $\hat{y}$ variation, which is reasonable if the initial condition has no such variation. This assumption makes the problem inherently linear, and disallows velocities normal to the boundary, i.e. $\hat{w} = 0$. Hence the solutions cannot represent the overturning of unstable stratifications. In geophysical boundary flows such overturning is often parameterized by increased eddy viscosity and diffusivity in the unstable region. For the purposes of our analysis we shall assume that ν and κ are constant, and simply point out where the solutions are not statically stable.

Writing the equations in the rotated frame of reference, and adding $\cos\alpha$ times the $\hat{x}$-momentum equation to $\sin\alpha$ times the $\hat{z}$-momentum equation to eliminate the pressure, we find

$$\frac{\partial \hat{u}}{\partial t} - f\cos\alpha(\hat{v} - V) = -B\sin\alpha + \nu\frac{\partial^2 \hat{u}}{\partial \hat{z}^2}, \tag{2.7a}$$

$$\frac{\partial \hat{v}}{\partial t} + f\cos\alpha\,\hat{u} = \nu\frac{\partial^2 \hat{v}}{\partial \hat{z}^2}, \tag{2.7b}$$

$$\frac{\partial B}{\partial t} = N^2\sin\alpha\,\hat{u} + \kappa\frac{\partial^2 B}{\partial \hat{z}^2}. \tag{2.7c}$$

We have written B for the buoyancy, $g\rho'/\rho_0$, to simplify the notation. The boundary conditions are

$$\hat{u} = \hat{v} = 0 \quad \text{at} \quad \hat{z} = 0, \tag{2.8a}$$

$$\frac{\partial B}{\partial \hat{z}} = N^2\cos\alpha \quad \text{at} \quad \hat{z} = 0, \tag{2.8b}$$

$$\hat{u} \quad \text{and} \quad B \to 0 \quad \text{as} \quad \hat{z} \to \infty, \tag{2.8c}$$

and

$$\hat{v} \to V \quad \text{as} \quad \hat{z} \to \infty. \tag{2.8d}$$

Thus there is a no-slip velocity boundary condition, and the slope is insulating. When $\kappa = 0$, (2.8*b*) should be replaced by

$$B = 0 \quad \text{at} \quad \hat{z} = 0. \tag{2.8e}$$

When $\alpha = 0$, (2.7) gives rise to a standard Ekman layer. When $N = 0$ the solution is a modified Ekman layer with thickness

$$\delta_s = (2\nu/f\cos\alpha)^{\frac{1}{2}}. \tag{2.9}$$

The subscript s indicates that this is in the slope frame of reference.

Buoyancy becomes important to the momentum balance through the term $B\sin\alpha$ in (2.7*a*), which grows in magnitude initially by advection of the stratification, and by diffusion of the boundary condition. For the non-diffusive ($\kappa = 0$) case we may simply estimate when buoyancy will first become important. Assuming that buoyancy is initially unimportant the solution will be approximately the modified Ekman layer of thickness δ_s described above. In the boundary layer we may then make the scale estimates:

$$(\hat{v} - V) \quad \text{and} \quad \hat{u} \sim -V. \tag{2.10}$$

Integrating (2.7*c*) in time and using the scale estimate, the buoyancy within the boundary layer is approximately

$$B \sim -VN^2\sin\alpha\,\tau_0, \tag{2.11}$$

at a time τ_0. Substituting this expression into the $\hat{x}$-momentum equation (2.7a) we find that the buoyancy term becomes as large as the Coriolis term when

$$\tau_0 \sim \frac{f\cos\alpha}{(N\sin\alpha)^2}. \tag{2.12}$$

The above derivation was based on the assumption that Ekman theory was workable for some time before buoyancy became important, which implies $(N/f)\tan\alpha \ll 1$. If this were not the case then buoyancy would presumably become important while the Ekman layer was forming. Walin (1969) suggests that Ekman-layer theory remains valid if $(N/f)\tan\alpha$ is small. Our scale analysis (and full theory to be presented below) in fact predicts that buoyancy forces eventually become substantial unless $(N/f)\tan\alpha$ is actually zero.

2.2. *Steady solutions*

Thorpe's (1987) steady solution to (2.7) subject to boundary conditions (2.8) is

$$\hat{u} = \frac{2\kappa\cot\alpha}{\delta_T}\exp(-\hat{z}/\delta_T)\sin(\hat{z}/\delta_T), \tag{2.13a}$$

$$\hat{v} = V_T(1-\exp(-\hat{z}/\delta_T)\cos(\hat{z}/\delta_T)), \tag{2.13b}$$

where

$$\delta_T = \left(\frac{4\nu^2}{(f\cos\alpha)^2+\sigma(N\sin\alpha)^2}\right)^{\frac{1}{4}}, \tag{2.14a}$$

and

$$V_T = -2(\kappa\cot\alpha)\,\delta_T/\delta_S^2. \tag{2.14b}$$

This solution has roughly the form of an Ekman layer of thickness δ_T. The subscript T is for Thorpe. The along-slope velocity in the interior is fixed by the density boundary condition to a constant value, V_T. The cross-slope transport is completely determined by the diffusivity and the slope angle, as seen by the integral

$$\int_0^\infty d\hat{z}\,\hat{u} = \kappa\cot\alpha. \tag{2.15}$$

This result, which comes directly from integration of the steady form of (2.7c), with boundary condition (2.8b), expresses the fact that for the steady problem there must be a global balance of advective and diffusive buoyancy fluxes. Thorpe also extends his solution to the case where the viscosity and diffusivity vary away from the slope, to represent flows with a mixed layer at the boundary. Still, it remains difficult to apply these solutions to geophysical situations where the along-slope velocity is arbitrary. Garrett (1990) has addressed this problem by suggesting that the thickness and diffusivity of the mixed layer may adjust to conform to the interior flow. He finds that it may be possible to have such a solution for arbitrary interior velocity V of positive sign.

Even if the diffusivity and viscosity are variable, steady solutions still strongly limit the cross-slope transport. Thorpe shows that the integrated transport in this case (still holding N constant) is always given by $\kappa_\infty\cot\alpha$, where κ_∞ is the value of κ as $\hat{z}\to\infty$. This would have drastic consequences for geophysical flows, through the fast spin-up process, if the steady solutions were always in force. Taking this as a caution about the applicability of steady solutions we shall explore the time-dependent case analytically below.

2.3. *Approximate unsteady solutions*

Consider a situation where, initially, $\hat{u} = B = 0$, and $\hat{v} = V$ everywhere except at the boundary. In the absence of stratification, an Ekman layer of thickness δ_s will develop in a time $O(\Omega^{-1})$. With stratification, buoyancy will become important in a time τ_0, (2.12).

Let us assume for the moment that the buoyancy has become sufficiently important that the along-slope velocity $\hat{v}$ has come approximately into 'thermal wind' balance with the density field. This would be expressed by an approximate version of the $\hat{x}$-momentum equation (note that (2.16) is actually a $\hat{z}$-integral of the thermal wind equation):

$$\frac{\hat{v}}{V} - 1 = B\frac{\sin\alpha}{Vf\cos\alpha} + O(R_t, E_s)\frac{U}{V}, \tag{2.16}$$

where U is the scale of the $\hat{u}$-velocity,

$$R_t = (\tau_u f\cos\alpha)^{-1}, \tag{2.17}$$

a temporal Rossby number, and

$$E_s = (\delta_s/D_u)^2, \tag{2.18}$$

an Ekman number. Here τ_u is the timescale of the temporal variations of $\hat{u}$, and D_u is the thickness of the boundary layer for $\hat{u}$. Below we shall be able to make more meaningful estimates of when and where these are small, and hence assess the validity of the thermal wind approximation in (2.16).

Assuming that R_t and E_s are negligibly small, we take $\partial/\partial t$ and $\partial^2/\partial\hat{z}^2$ of (2.16) and substitute the results into the buoyancy equation (2.7*c*) to find

$$\frac{f\cos\alpha}{\sin\alpha}\frac{\partial\hat{v}}{\partial t} = N^2\sin\alpha\,\hat{u} + \kappa\frac{f\cos\alpha}{\sin\alpha}\frac{\partial^2\hat{v}}{\partial\hat{z}^2}. \tag{2.19}$$

Solving this for $\hat{u}$ and substituting into the $\hat{y}$-momentum equation (2.7*b*) the result may be written as

$$\frac{\partial\hat{v}}{\partial t} = \nu\left(\frac{1/\sigma + S}{1+S}\right)\frac{\partial^2\hat{v}}{\partial\hat{z}^2}, \tag{2.20}$$

where

$$S = \left(\frac{N\sin\alpha}{f\cos\alpha}\right)^2, \tag{2.21}$$

a Burger number. Thus the along-slope momentum dynamics have been reduced to a simple diffusion equation, despite the presence of both rotation and stratification. We shall refer to (2.20) as the 'slow diffusion' equation, since for $\sigma > 1$ it predicts that the boundary layer will diffuse inward more slowly than the usual non-rotating boundary layer. The cross-slope flow leads to Coriolis forces which oppose the diffusion of along-slope momentum into the fluid. This is the effect that slows the diffusion and, in the case of an Ekman layer, brings it to a halt. Yet the growing buoyancy force does not allow a steady Ekman balance, and so the boundary layer continues to thicken.

The slow-diffusion equation (2.20) is, in the limit $S \ll 1$ (and $S \sim O(1/\sigma)$), identical to a result derived previously by Gill (1981) for the evolution of the density field during the spin-down of a frontal region in the ocean interior (see also Garrett 1982). In their context slow diffusion is seen as an enhanced lateral diffusion.

Using the slow-diffusion equation (2.20) we may also estimate the cross-slope transport. Taking the $\hat{z}$-integral of the buoyancy equation (2.7*c*) and applying the insulating boundary condition (2.8*b*) we form

$$\int_0^\infty \mathrm{d}\hat{z}\frac{\partial B}{\partial t} = MN^2\sin\alpha - \kappa N^2\cos\alpha, \tag{2.22}$$

where

$$M = \int_0^\infty \mathrm{d}\hat{z}\,\hat{u}, \tag{2.23}$$

the cross-slope transport. Substituting $\hat{v}$ for B as before from the approximate thermal wind equation (2.16) (with R_t and E_s equal to zero) and rearranging we find

$$M = \frac{1}{Sf\cos\alpha}\int_0^\infty \mathrm{d}\hat{z}\frac{\partial\hat{v}}{\partial t} + \kappa\cot\alpha. \tag{2.24}$$

Hence, if the flow does attain a steady state, the cross-slope transport is given by Thorpe's result (2.15). Assuming that the slow-diffusion equation (2.20) adequately describes the time rate of change of $\hat{v}$ over most of the boundary layer, we may use it to obtain a scale estimate of the integral term in (2.24). By time t, $\hat{v}$ will have changed by an amount comparable with $-V$ (assuming $\hat{v}=0$ is the proper bottom boundary condition for (2.20)) in a region of thickness D_v estimated from (2.20) as

$$D_v \sim \left[\nu t\left(\frac{1/\sigma+S}{1+S}\right)\right]^{\frac{1}{2}}. \tag{2.25}$$

Hence we may form the scale estimate

$$\int_0^\infty \mathrm{d}\hat{z}\frac{\partial\hat{v}}{\partial t} \sim D_v\left(\frac{-V}{t}\right). \tag{2.26}$$

Using this result the transport equation may be rewritten as

$$\frac{M}{|M_0|} = C\left(\frac{\tau}{t}\right)^{\frac{1}{2}} + \frac{\kappa\cot\alpha}{|M_0|}, \tag{2.27}$$

where

$$\tau = \frac{1}{S^2 f\cos\alpha}\left(\frac{1/\sigma+S}{1+S}\right). \tag{2.28}$$

We shall call τ the 'shut-down time' because it gives the timescale over which the cross-slope transport relaxes to the steady limit of Thorpe's solution, $\kappa\cot\alpha$. C is an $O(1)$ constant to be determined empirically. We have normalized the equation by $|M_0| = |-\frac{1}{2}V\delta_s|$, the magnitude of the steady Ekman transport when $N=0$, since this will be the scale of the transport before buoyancy becomes important.

For $\sigma=\infty$ and $S\ll 1$ the shut-down time, τ, is equal to τ_0, the timescale we determined in (2.12) for the onset of buoyancy effects in the boundary layer. Thus, at least for this simple case, the shut-down time is the time it takes for cross-slope advection to significantly alter the force balance within the boundary layer.

When $\sigma=1$ the shut-down time varies as α^{-4}, indicating that care should be taken when applying the theory to regions of non-constant slope. In particular, the horizontal lengthscale of variation in τ should be much greater than the boundary-layer thickness.

The analysis above hinged upon having very small values of R_t and E_s, the scales of the inertial and viscous terms in the $\hat{x}$-momentum equation (2.16). While the boundary layer is initially forming, the timescale for changes in $\hat{u}$ will be $(f\cos\alpha)^{-1}$, and R_t will be $O(1)$, so clearly our results do not apply for this early time. After this

time the transport equation (2.27) suggests that the timescale for changes in $\hat{u}$ will be τ, the shut-down time. Thus we expect $R_t \ll 1$ if (i) $t \gg (f\cos\alpha)^{-1}$, and (ii) $\tau \gg (f\cos\alpha)^{-1}$. We shall see in §3 that violation of this constraint on τ does not significantly alter our results. The viscous term E_s will also initially be at least $O(1)$ for $t < (f\cos\alpha)^{-1}$, since the boundary layer is thinner than δ_s before that time. If the boundary layer for $\hat{u}$ later thickens at the same rate as slow diffusion (2.20) predicts for $\hat{v}$ then E_s will be small when $D_v \gg \delta_s$. In general we expect that $E_s \ll 1$ if (i) $t \gg (f\cos\alpha)^{-1}$, and (ii) $D_u \gg \delta_s$. We explore the validity of these expectations numerically below.

3. Numerical solutions

The set of coupled equations (2.7) describing the boundary layer was solved numerically, using forward-differencing in time, and central-differencing in space. Each run was initialized with $\hat{u}$ and $\hat{v}$ set equal to the steady $N = 0$ Ekman-layer solution on a slope, and with $B = 0$. This was done to minimize inertial oscillations in the solutions, similar to the gradual 'switching on' of the boundary condition as seen, for example, in Weatherly & Martin (1978). We are thus necessarily concentrating only on boundary-layer behaviour for $t > (f\cos\alpha)^{-1}$. Runs started with undisturbed initial conditions, $\hat{u} = 0$, $\hat{v} = V$, and $B = 0$, had the same general behaviour as the solutions shown below, but had larger inertial oscillations, making the results more difficult to see. There were approximately six grid points within the initial boundary-layer thickness, δ_s (typically 0.14 cm), and 2400 time steps per period of revolution. Integrations covered a depth of at least $70\delta_s$, and the boundary layer never significantly interacted with the upper boundary. The numerical scheme was checked against known behaviour (e.g. final steady velocity profiles, and timescale for decay of transients) of the unstratified case.

3.1. *Numerical integrations with little or no diffusivity*

Our laboratory experiments were salt stratified, so density diffusion was essentially negligible over the timescales of interest. To compare with these experiments we first present results of numerical integrations for the case $\kappa = 0$. Throughout all the numerical results, $f = 1\ \mathrm{s}^{-1}$, $N = 2\ \mathrm{s}^{-1}$, and $\nu = 0.01\ \mathrm{cm}^2\ \mathrm{s}^{-1}$, values typical of the laboratory experiments.

Figure 1 (*a*) shows $\hat{u}$- and $\hat{v}$-profiles versus $\hat{z}$ at three different dimensionless times for $V = -1\ \mathrm{cm\ s}^{-1}$ (corresponding to up-slope boundary-layer transport). Note that the $V = \pm 1\ \mathrm{cm\ s}^{-1}$ solutions are symmetrical in their velocity fields. The dashed lines are solutions to the slow diffusion equation (2.20) at the same times (also initialized with the steady $N = 0$ Ekman velocity profile, and with a no-slip lower boundary condition). The $\hat{v}$ boundary layer thickened almost exactly as predicted by the slow diffusion equation, especially for large t/τ. The up-slope flow decreased in magnitude over time, and extended over roughly the same thickness as the $\hat{v}$ boundary layer. In this instance, lacking density diffusion, it was the cross-slope velocity $\hat{u}$ that had to advect the density field to bring $\hat{v}$ into thermal wind balance. The accuracy of the slow diffusion equation in predicting the $\hat{v}$-velocity is an indication that the thermal wind assumption was valid over almost the whole depth of the boundary layer, particularly for larger t/τ (inspection of the individual terms in (2.7*a*) during the integration also showed this to be true).

As $\hat{u}$ advects the stratification up- or down-slope, there is the clear possibility that the resulting density field may not be statically stable. Figure 1 (*b*) shows the density

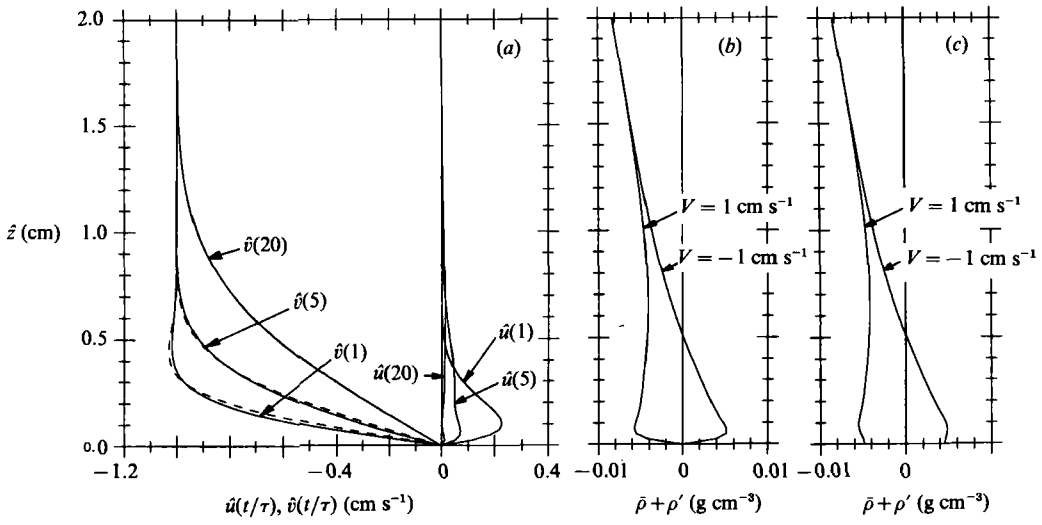

FIGURE 1. Numerical solutions of (2.7) versus $\hat{z}$, with $\alpha = 10°$, $f = 1\ \mathrm{s}^{-1}$, $N = 2\ \mathrm{s}^{-1}$, and $\nu = 0.01\ \mathrm{cm}^2\ \mathrm{s}^{-1}$. Along-slope ($\hat{v}$) and cross-slope ($\hat{u}$) velocity profiles are shown in (*a*) for $\kappa = 0$ and $V = -1\ \mathrm{cm\ s}^{-1}$, at three dimensionless times: $t/\tau = 1$, 5, and 20 ($\tau = 7.3$ s). The $\hat{v}$-profiles are compared with solutions (dashed lines) of the slow-diffusion equation (2.20) for the same times (at $t/\tau = 20$ the profiles are nearly identical). The density perturbation, $\bar{\rho}+\rho'$, at $t/\tau = 20$ is shown in (*b*) with all parameters as in (*a*) except that $V = \pm 1\ \mathrm{cm\ s}^{-1}$. The effect of a small density diffusivity, $\kappa = 10^{-5}\ \mathrm{cm}^2\ \mathrm{s}^{-1}$, on the profiles in (*b*) is shown in (*c*).

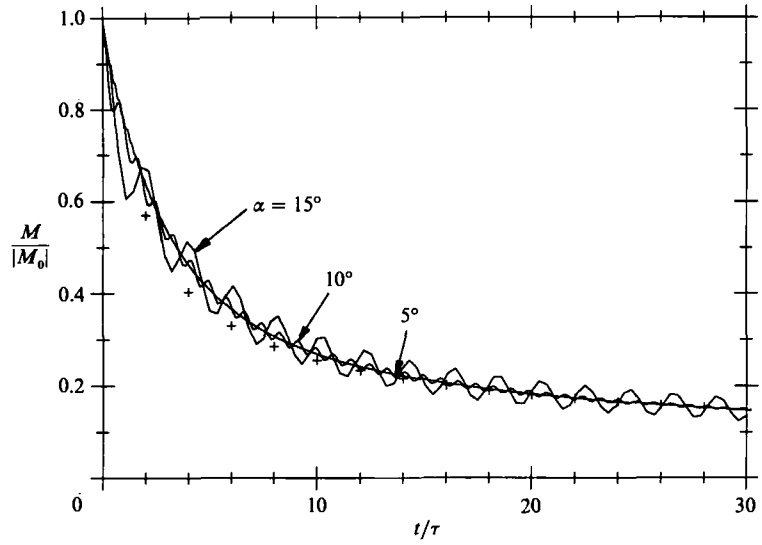

FIGURE 2. Normalized cross-slope transport versus t/τ from three numerical solutions to (2.7). All parameters were as in figure 1 (*a*) except the slope angle, which was varied as shown. Also shown (+) is a fit to the data given by $M/|M_0| = 0.8072\ (t/\tau)^{-\frac{1}{3}}$.

perturbation, $\rho+\rho'$, at $t/\tau = 20$, for two different interior along-slope velocities, $V = +1\ \mathrm{cm\ s}^{-1}$ (causes a down-slope transport), and $V = -1\ \mathrm{cm\ s}^{-1}$ (causes an up-slope transport). Figure 1 (*c*) shows the density perturbation for the same situations as in (*b*) except with $\sigma = 10^3$, representative of the actual molecular diffusivity of salt. The up-slope favourable case ($V = -1\ \mathrm{cm\ s}^{-1}$) was statically unstable only in a

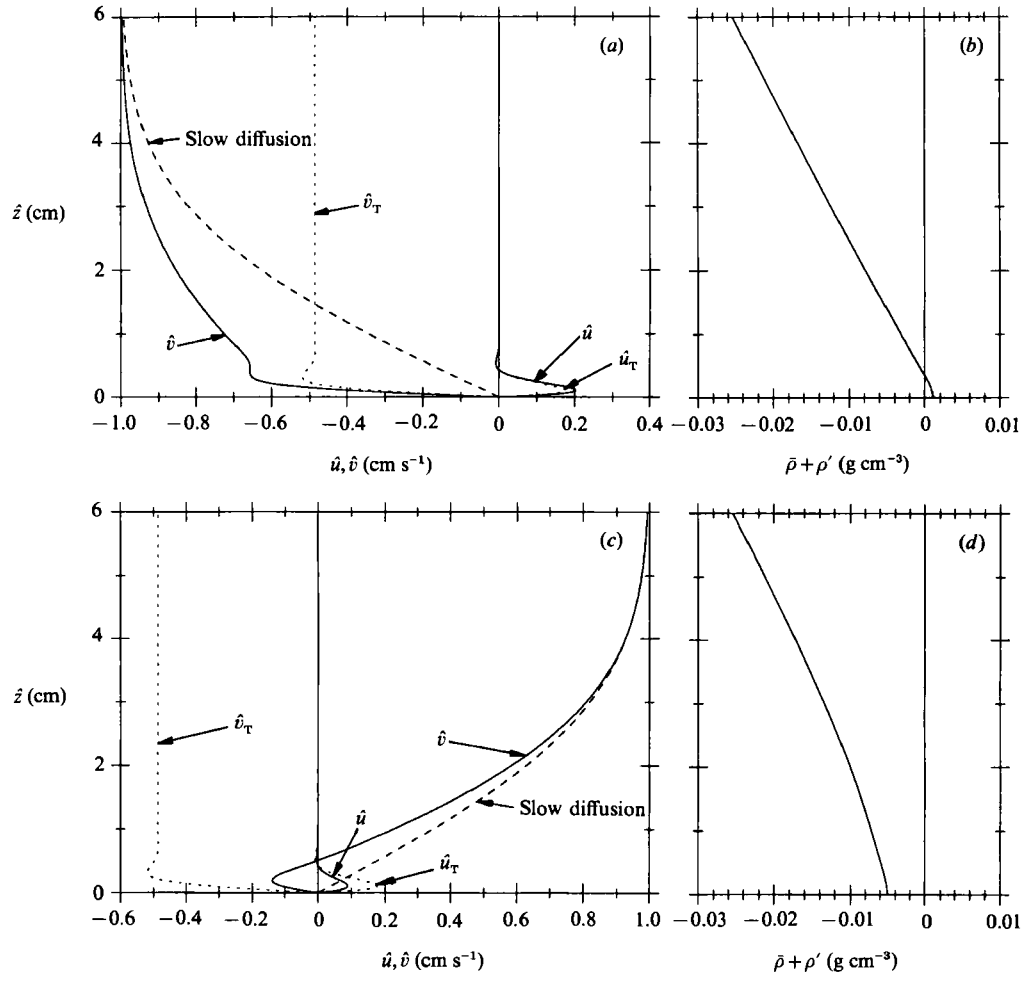

FIGURE 3. Numerical solutions of (2.7) versus $\hat{z}$, with $\alpha = 15°$, $f = 1$ s^{-1}, $N = 2$ s^{-1}, and $\nu = \kappa = 0.01$ cm^2 s^{-1}; all at $t/\tau = 20$ ($\tau = 12.6$ s). In (*a*) and (*b*) $V = -1$ cm s^{-1}, whereas in (*c*) and (*d*) $V = 1$ cm s^{-1}. The $\hat{v}$-profiles are compared with solutions (dashed lines) of the slow diffusion equation (2.20). Also shown (dotted lines, marked $\hat{u}_T$ and $\hat{v}_T$) are the $\hat{u}$- and $\hat{v}$-profiles for Thorpe's steady solution (2.13) with the same parameters (except V).

region very close to the boundary, and most of this unstable region was removed by the small diffusivity. In all of the laboratory experiments presented below this was the sense of the interior velocity field, hence we ignore static instability in our analysis of the experiments. By contrast, the down-slope case ($V = +1$ cm s^{-1}) was marginally unstable over much of the boundary layer, and the diffusivity did little to change this situation. Thus we expect that for $\sigma \gg 1$ our theory may need to be modified for interior velocities of positive sign, to account for possible static instability. Indeed, some laboratory experiments (not presented here) involving down-slope flow did show signs of instability in the boundary layer.

Figure 2 shows the normalized cross-slope transport $M/|M_0|$, versus non-dimensional time t/τ, for runs with three different slope angles, $\alpha = 5°$, $10°$, and $15°$, with corresponding shut-down times 31.8, 7.3 and 2.8 s. For these runs $\kappa = 0$ and $V = -1$ cm s^{-1}. All other parameters were as before. The three curves collapsed to one

(except for the inertial oscillations), indicating that τ was the correct parameter to non-dimensionalize the time. Also plotted (+) is a fit to the curves based on our transport prediction (2.27). The constant C we used was 0.8072, which came from fitting (2.27) to the numerical data at $t/\tau = 30$. The fit looks good, even as early as $t/\tau = 2$, indicating that, at least for $\kappa = 0$, the transport resembles our prediction.

When $\alpha = 15°$, $\tau = 2.8$ s, and so we would expect buoyancy effects to become important even before the Ekman layer is fully set up, possibly violating the scaling requirement $\tau \gg (f\cos\alpha)^{-1}$. The only noticeable effect of this short τ, however, was to excite somewhat larger inertial oscillations than in the cases with longer τ.

3.2. *Numerical integrations with large diffusivity*

Subsequent numerical runs were carried out with $\kappa = \nu = 0.01$ cm^2 s^{-1} ($\sigma = 1$) to explore the effects of large density diffusion upon the boundary layer. Again, $f = 1$ s^{-1}, and $N = 2$ s^{-1}. For all runs the slope was 15°. The only parameter that was varied was the sign of the initial interior velocity, V, being either plus or minus 1 cm s^{-1}.

Figure 3 (*a*, *c*) shows $\hat{u}$- and $\hat{v}$-velocity profiles versus $\hat{z}$ at $t/\tau = 20$ ($\tau = 12.6$ s) for (*a*) $V = -1$ cm s^{-1}, and (*c*) $V = +1$ cm s^{-1}. Plotted as dashed lines are solutions to the slow diffusion equation at the same time. For comparison the $\hat{u}$- and $\hat{v}$-velocities for Thorpe's steady solution with the same parameters (except V, which we are not free to specify) are plotted as dotted lines. In both cases the $\hat{v}$-velocity profile had diffused away from the boundary approximately as much as the slow-diffusion solution predicted, but the magnitude of the $\hat{v}$-velocity did not match the slow-diffusion solution, especially near the boundary. The $\hat{u}$-velocity had become positive in both cases by this time, and was concentrated near the boundary in a Thorpe-like profile. In these cases the assumption of thermal wind balance in $\hat{v}$ was probably flawed close to the boundary, owing to the density boundary condition. Specifically, the Ekman number, E_s, had probably become large there owing to the thinness of D_u.

The stratification parameter, $\bar{\rho}+\rho'$, is shown at the same time, for these two cases in figure 3 (*b*, *d*). In both cases the stratification remained statically stable because of smoothing by the density diffusion. The perturbation to the mean stratification diffused upwards approximately as far as the $\hat{v}$-velocity profiles. In contrast to the $\kappa = 0$ cases, here diffusion was the primary means of altering the density, except near the boundary where $\hat{u}$ remained large.

Figure 4 (*a*) shows two families of $\hat{v}$-velocity profiles (with parameters as in figure 3) over a long period of time. The profiles suggest strongly that the time-dependent solution is moving toward Thorpe's steady solution. The $\hat{u}$-velocity may achieve this goal fairly easily since it is concentrated near the boundary, but the $\hat{v}$-velocity must change everywhere to attain the steady solution. This then appears to be the role of slow diffusion: the gradual transformation of the interior along-slope flow to that of Thorpe's steady solution, V_T. In addition, the numerical solutions imply that V_T is eventually the correct bottom boundary condition for the slow-diffusion equation, not $\hat{v} = 0$ as we used. When $\kappa = 0$, V_T is also zero, which explains why the slow-diffusion solution was so accurate in that case (figure 1).

The normalized cross-slope transport for the two runs of figure 3 is plotted versus t/τ in figure 4 (*b*). Also plotted (+) are fits to the runs. The fits are from

$$\frac{M}{|M_0|} = C\frac{(M_0 - (\kappa\cot\alpha)\,\delta_T/\delta_s)}{|M_0|}\left(\frac{\tau}{t}\right)^{\frac{1}{2}} + \frac{\kappa\cot\alpha}{|M_0|}, \tag{3.1}$$

which was derived in exactly the same manner as (2.27), but using the idea,

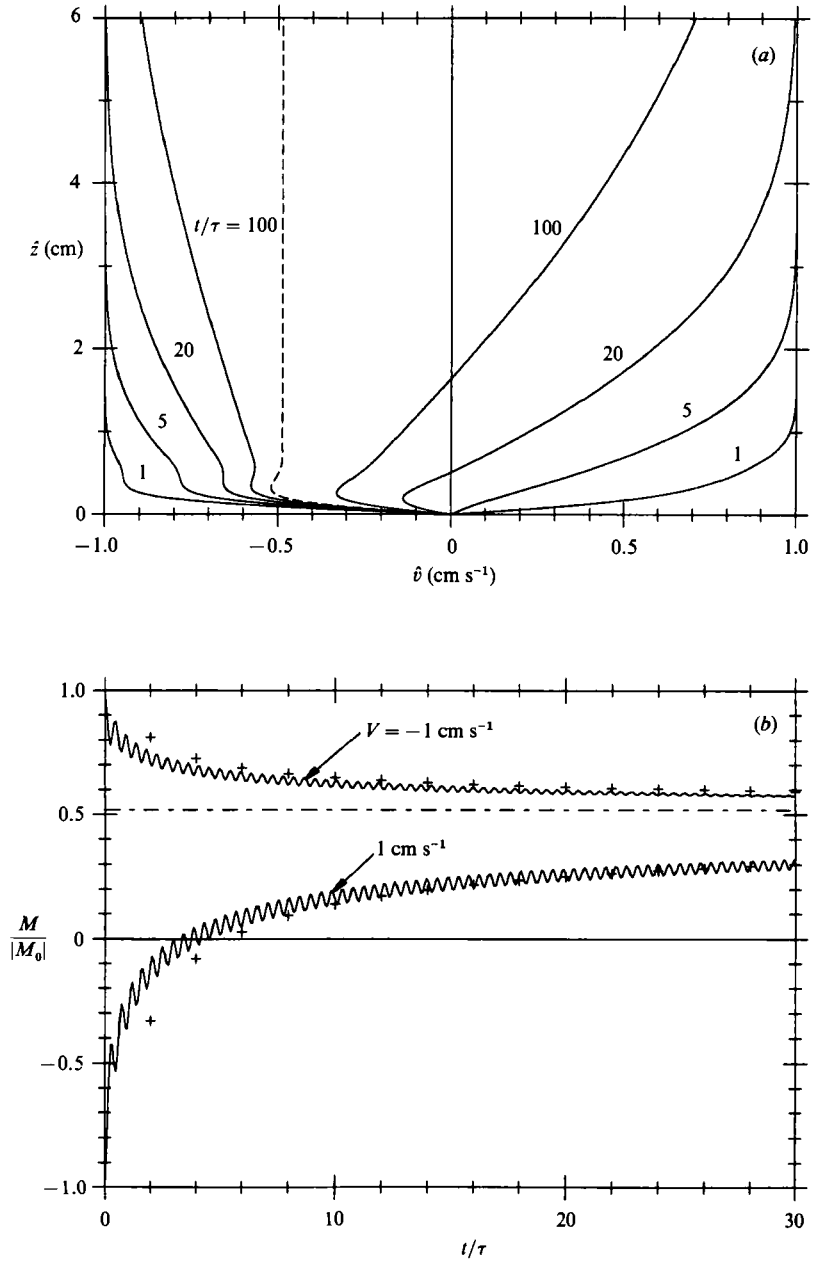

FIGURE 4. (*a*) Numerical solutions for $\hat{v}$ at different times (times shown are non-dimensionalized by τ), with parameters as in figure 3. Thorpe's steady solution for $\hat{v}$ is also shown (dashed line). Profiles to the left of the dashed line had $V = -1$ cm s^{-1}, and those to the right had $V = 1$ cm s^{-1}. Normalized cross-slope transport versus t/τ is plotted in (*b*) for two numerical solutions to (2.7). All parameters were as in figure 3. Also shown (+) are fits to the data based on (3.1). The limiting value of the (normalized) transport, $\kappa \cot\alpha/|M_0|$, is also shown (dashed line).

suggested by the numerical solutions, that V_T is eventually the proper bottom boundary condition for the slow diffusion equation. Hence instead of scaling $\partial\hat{v}/\partial t$ as $-V/t$, we used $\partial\hat{v}/\partial t \sim -(V-V_T)/t$. This should somewhat overestimate the magnitude of $\partial\hat{v}/\partial t$, since the assumed bottom boundary condition was actually only

gradually achieved, and this was the sense of the error in the plotted fits. Note that the analysis in §2 is unable to determine the rate at which this new bottom boundary condition is established. The fits used the same empirical constant, $C = 0.8072$, as was determined from the $\kappa = 0$ case, and are still fairly good, especially at larger t/τ.

The theoretical ideas of §2 and the above numerical simulations support the conclusions that: (i) the $\hat{v}$ boundary layer diffuses into the interior at a rate predicted by the slow-diffusion equation, eventually bringing $\hat{v}$ in the interior to V_T, and (ii) the cross-slope transport changes from M_0 to $\kappa \cot \alpha$ over time as $(t/\tau)^{-\frac{1}{2}}$.

4. Experimental set-up

Laboratory experiments were carried out on a rotating table at the CSIRO Marine Laboratories in Tasmania, Australia. Rotation speed was controlled to within ± 0.001 rad s^{-1}. The main tank (figure 5) used in these experiments was a Plexiglas section of a sphere. It varied from axial symmetry by no more than ± 0.25 cm. This tank will be referred to as 'the bowl'. For comparison we also did experiments in a right-circular cylindrical tank, 45.5 cm in radius and filled to the same depth as the bowl.

The tank was stratified with salt, hence density diffusion was almost non-existent over the course of an experiment. Typically the tank was stratified in five layers of increasingly salty water, from 0 to 140 parts per thousand, giving a nominal 10% density difference from top to bottom. The kinematic viscosity also varied by about 10% owing to the salinity, and account was taken of this variation in the analysis, §6. The layers were allowed to diffuse to a smooth profile overnight. Density was measured with a profiler that recorded conductivity, temperature and depth. The profiler had a spatial resolution of about 0.2 cm vertically. Typical profiles of density, ρ, and buoyancy frequency, N, are shown in figure 6. N goes to zero near the top and bottom owing to density diffusion. The profile shown is from the centre of the bowl. Profiles of N taken away from the centre do not go to zero near the lower floor except in a very small diffusive boundary layer. Previous experimenters have gone to great lengths (see for example Buzyna & Veronis 1971) to achieve a constant N-profile so that they could compare their experimental results with theory. For our experiments we shall make local comparisons of the flow with the theory developed in §2, so a local knowledge of N and α is sufficient. The centre of the bowl almost unavoidably had a small pool of low-N water at the bottom, and the dynamics there were generally very different from those at greater radius where N and α conspired rapidly to make buoyancy important in the boundary layer. Our comparisons are based on the assumption that the two regions did not interact significantly. This will be discussed further in §6.

For a typical experiment the fluid was stratified and allowed to spin-up overnight, with a lid on top to avoid air stress at the surface. The lid was 3 cm above the surface of the water. At $t = 0$ the rotation rate of the container was increased by an amount $\Delta\Omega$ (approximately 10%), over about 5 s. Initially the fluid was in solid-body rotation relative to the container, which was the new frame of reference, at an angular velocity $-\Delta\Omega$ (for a spin-up). The Rossby number, ϵ, of the flow is given by $\epsilon = \Delta\Omega/\Omega$. For small ϵ forcing along the boundary at lengthscale L will penetrate a depth H_P into the fluid, where $H_P = fL/N$. For our experiments f/N was around 1/3 in the body of the fluid, whereas the aspect ratio, depth/radius, of our containers was around 1/4. So we expected that the effects of boundary forcing would extend to the surface of the fluid, although showing some noticeable attentuation by then.

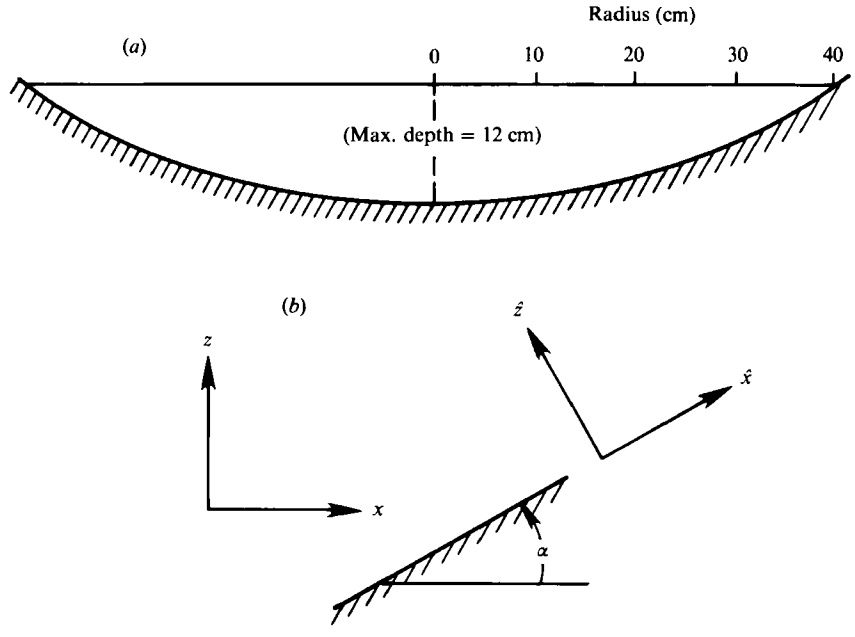

FIGURE 5. (*a*) Cross-section of the 'bowl' used in the laboratory experiments, and (*b*) a definition sketch of the slope coordinate frame.

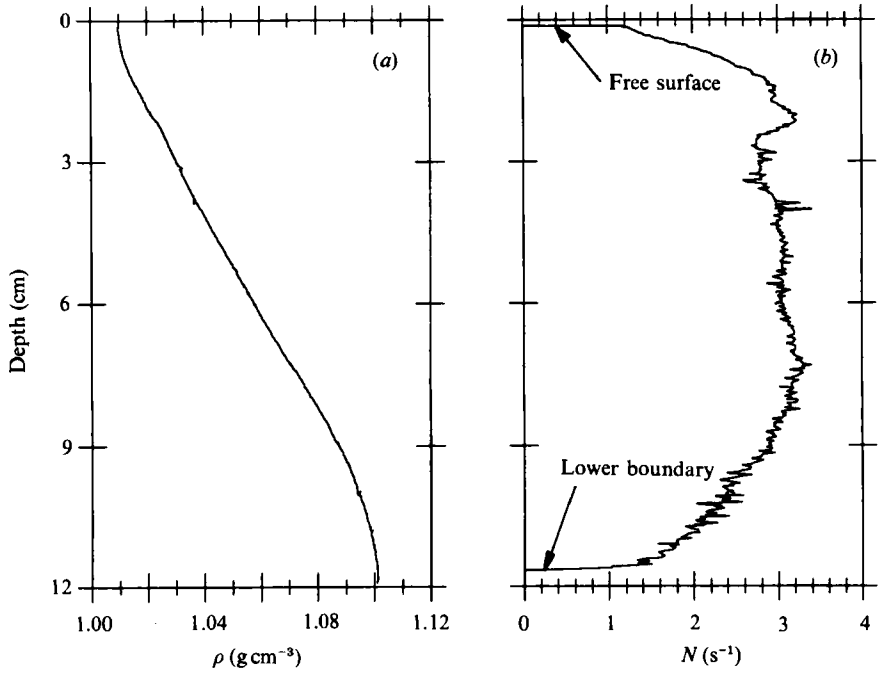

FIGURE 6. Measured profiles of (*a*) density and (*b*) buoyancy frequency versus depth, at the centre of the bowl, for a typical laboratory experiment.

Various flow visualization techniques, described in §5, allowed us to track the fluid as it eventually spun-up to the new rotation rate of the container. Density profiles were taken before and after experiments, and in general were nearly indistinguishable.

Although we present the laboratory experiments as support for the theoretical ideas of §2, in fact the laboratory work was done first, and served as a guide for the theory, which was developed later.

5. Experimental results

We used three types of flow visualization to explore spin-up in the stratified bowl and cylinder: (i) placing dye in the boundary layer to show the direction of stress at the wall, (ii) following beads floating on an isopycnal to determine zonal velocities (zonal is defined as along a circumference), and (iii) placing dye in the body of the fluid to show the shear history of the flow.

5.1. *Boundary-layer visualization*

To visualize flow in the boundary layer, just before a spin-up experiment a number of potassium permanganate crystals were dropped onto the bottom of the tank, along a radius. These exude a thick purple dye showing the direction of flow just above the bottom, and hence the direction of stress at the boundary. Figure 7 (*a*, *b*) shows these dye streaks during an experiment in the cylinder, and figure 7 (*c*, *d*) shows dye streaks for a similar experiment in the bowl. Both containers had similar stratifications.

Flow in the boundary layer of the cylinder remained very much like an Ekman layer, moving out and downstream at 45° to the local radius. This behaviour continued even as the interior flow was decreased by the fast spin-up. The bowl exhibited very different behaviour. Flow in the outer half of the tank, where α is greater and the shut-down time was very short, soon became mostly zonal, suggesting that the Ekman boundary layer was shut-down by the buoyancy forces on the sloping bowl wall. For this experiment τ was less than 5 s everywhere outside of $r = 15$ cm.

5.2. *Flow velocity measurements*

In order to measure zonal velocity we made long-exposure photos of particles ('beads') moving along density surfaces, similar to the technique used by Holton (1965). The beads were made of candle-wax and crayon, which could be combined in any ratio to conform even to the rather high densities near the bottom of our stratifications. A heated mixture of the two was sucked into a large syringe and then dotted out onto a flat surface to solidify in drops about 2 mm in diameter. The advantage of these beads is that they may be used for larger velocities than the thymol-blue technique (Buzyna & Veronis 1971). Also they give information on an entire density surface, instead of at just one point as in laser-Doppler velocimetry. The disadvantages are that it is difficult to make beads of perfectly consistent density, and the data reduction is somewhat time consuming. In a given experiment we had up to 60 beads floating along one density surface, with a vertical scatter in their positions of up to ± 0.5 cm. This led to some scatter in the velocity profiles in regions of strong vertical shear, and was the largest source of error in the data. Degassed water was used to avoid bubble formation on the bead surfaces.

With a group of light-coloured beads floating along an isopycnal, the room was

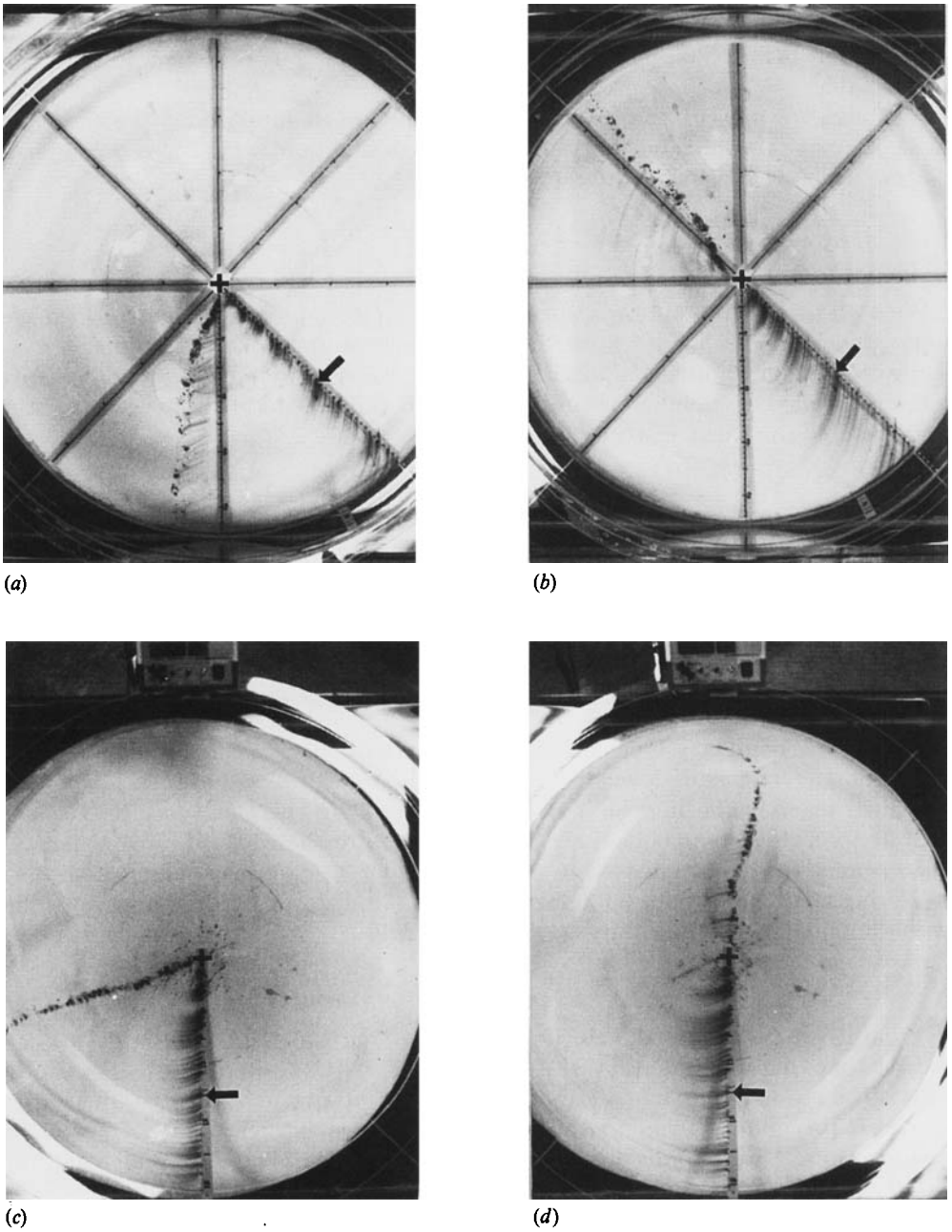

FIGURE 7. Photos of potassium permanganate in the boundary layer of two stratified spin-up experiments. The upper photos are looking down on the cylinder at (*a*) $t = 10$ s, and (*b*) $t = 40$ s. The lower photos show the bowl at (*c*) $t = 10$ s, and (*d*) $t = 40$ s. Crosses mark the centres, and the arrows point at $r = 25$ cm along the radius where the dye crystals lay. Both experiments were spun-up 15% from $f = 1$ s^{-1}. Radially outward flow persisted in the cylinder, yet it quickly disappeared in the bowl, especially at larger radius. Note the shape of the surface velocity profiles, indicated by the line of dye from very small crystals which dissolved immediately as they entered the water.

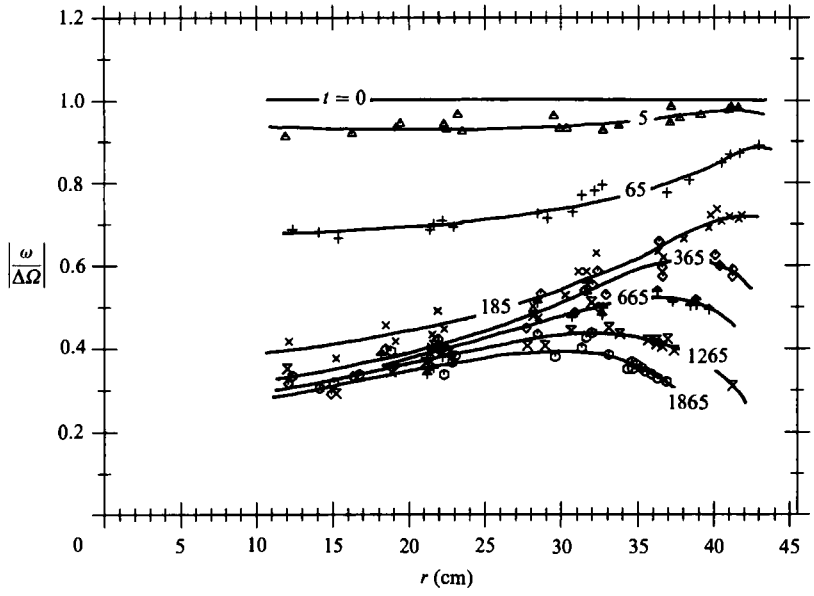

FIGURE 8. Normalized angular velocity versus radius, r, for a stratified spin-up experiment in the cylinder at a depth of 7 cm from the top (total depth was 11.6 cm), at eight different times (in seconds), as listed. The container was spun-up 15% from $f = 1.1$ s^{-1}. The solid lines are hand-drawn fits to the data. The fluid rapidly spun-up in the central region, which could be reached by the meridional circulation initially emanating from the outer corner.

darkened and a spin-up experiment initiated. The beads were lit by a strobe light, and were photographed from above in the rotating frame of reference. Each exposure spanned 10–20 flashes of the strobe, hence each bead would appear in a photo as a series of dots along an arc about the centre of the tank. Each photo gives a profile of angular velocity as a function of radius, at a given depth and time (the time was approximated as being midway through a photograph).

Figure 8 shows the time-history of the angular velocity, ω, for a 15% spin-up experiment in the stratified cylinder. The $t = 0$ line was drawn using the known $\Delta\Omega$ of the experiment. Within three minutes most of the fluid had been spun-up to about 55% of the new rotation rate. This was the signature of 'fast' spin-up in the cylinder, caused by vortex stretching driven by Ekman transport in the bottom boundary layer. Only over much longer times did the viscous boundary layer from the side and bottom walls begin to complete the spin-up to the new rotation rate. This region of 'fast' spin-up is qualitatively in agreement with previous theoretical and experimental work such as Walin (1969), and Buzyna & Veronis (1971). Notice the jet-like region near the outer boundary, which occurs in a region 'missed' by the meridional circulation.

Although there is some vertical displacement of density surfaces during 'fast' spin-up owing to vortex stretching, the density surfaces slump back almost to their initial positions over the longer viscous timescale. There is a tiny shift in isopycnals in the long term to fit the geopotential paraboloid of the new rotation rate, but this requires no vortex stretching. Ultimately, fluid particles in the interior achieve the new rotation rate because their potential vorticity has been altered by viscous stress.

Figure 9 shows a similar angular velocity history for a spin-up at two levels in the stratified bowl, starting from $f = 0.66$ s^{-1}. In this experiment there was little, if any,

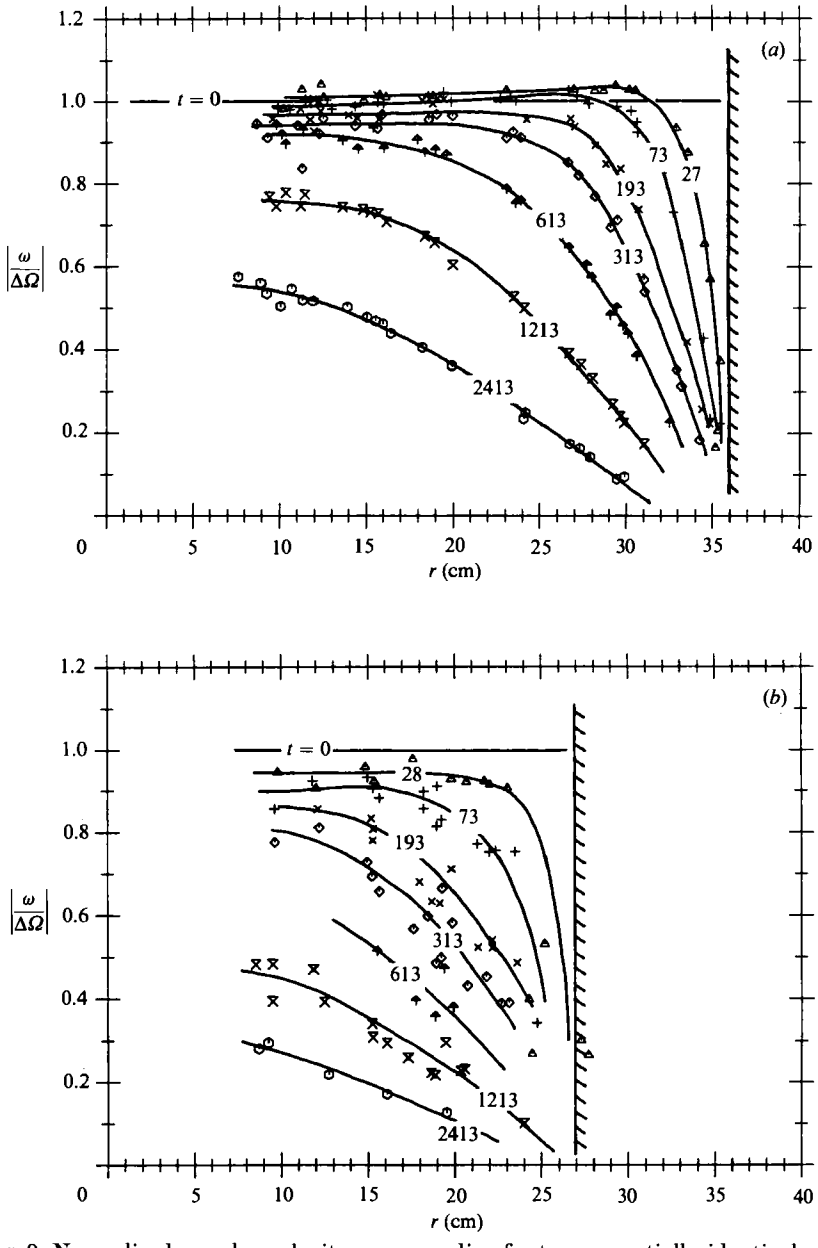

FIGURE 9. Normalized angular velocity versus radius for two, essentially identical, stratified spin-up experiments in the bowl at depths of (*a*) 3.4 cm from the top, and (*b*) 7.45 cm from the top (total depth at the centre was 11.7 cm), at eight different times (in seconds), as listed. The container was spun-up 10% from $f = 0.66\ \mathrm{s}^{-1}$. The edge of the tank at the given depth is marked with cross-hatching. The fluid adjusted slowly to the new rotation rate, and did so mainly by diffusion inward from the bottom. The early profiles in (*a*) indicate that a slight zonal circulation was present at the start of the experiment.

evidence of a 'fast' spin-up such as in the stratified cylinder. Presumably much of the Ekman layer had been shut-down by buoyancy forces, so the meridional circulation which causes 'fast' spin-up never developed.

Figure 10 is for a case similar to figure 9, except that $f = 1.5\ \mathrm{s}^{-1}$. In this experiment

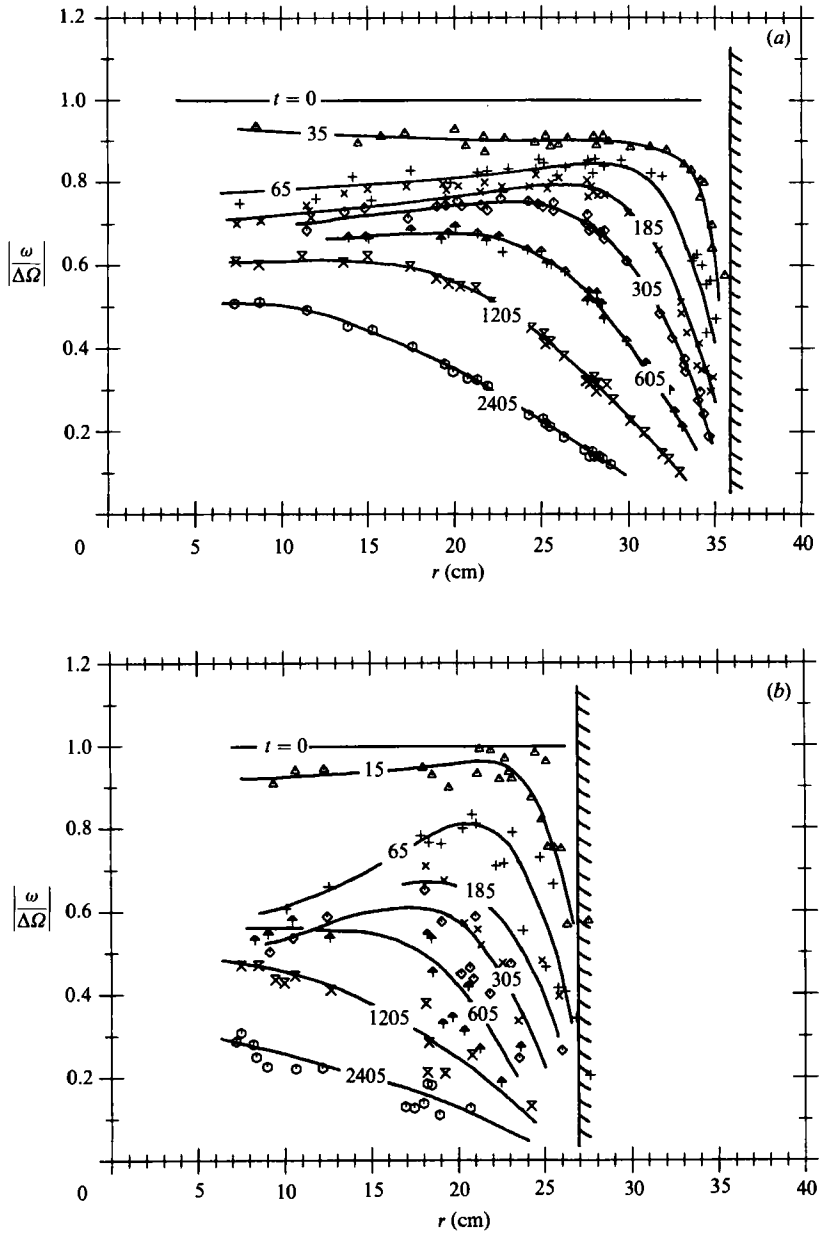

FIGURE 10. Same as figure 9 except the bowl was spun-up from $f = 1.5\ \mathrm{s}^{-1}$. There was clear evidence of some 'fast' spin-up in the acceleration of the inner region over the first minute. As in the cylinder, a zonal differential jet occurred in the corner where the meridional circulation had not reached.

there was some evidence of 'fast' spin-up. Recall that the shut-down time (2.28) increases with increasing f. In this case it appeared that the Ekman layer was operative long enough to affect the inner 15 cm of the flow, over the first minute. This issue will be taken up more quantitatively in §6.

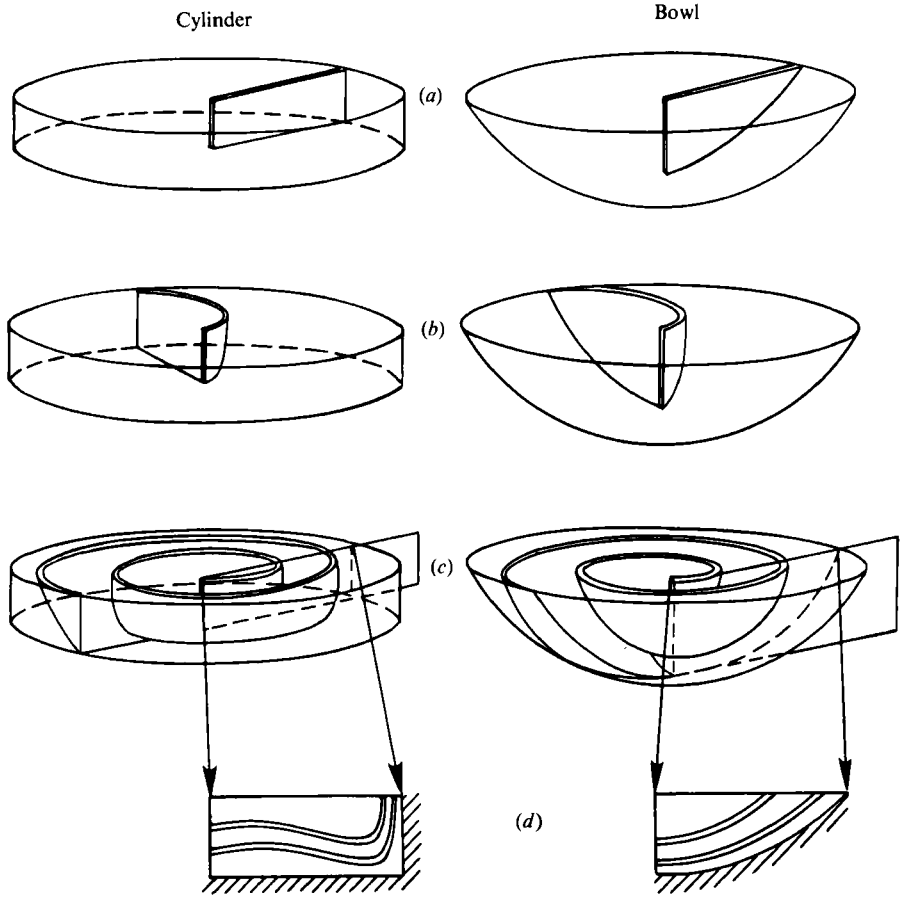

FIGURE 11. Onion-slice flow visualization in the stratified cylinder or bowl. Just before a spin-up experiment a sheet of dye (*a*) was injected into the fluid from top to bottom along a radius. As the spin-up started, (*b*), the dye sheet was stretched around the tank. As the spin-up proceeded, (*c*), the dye sheet was wrapped up into a spiral. A slice (*d*) through the dye sheet revealed lines of constant angular displacement. Fluid particles on adjacent dye lines in the slice had gone around the tank a complete revolution relative to each other.

5.3. *Onion-slice flow visualization*

One final method was used to see the 'shear history' of an experiment. A vertical plane of fluorescein dye was introduced with a 'rake' of injection tubes. Following figure 11, one can see how this dye plane is deformed by the sheared zonal velocity field. Slicing through this structure we find the dye lying along lines of constant angular displacement, with fluid particles on adjacent lines having travelled around the tank one revolution relative to each other. The slice was made by shining a sheet of light vertically down through the tank, so the dye lines appeared white on a dark background. We call this flow visualization technique an 'onion-slice' because of its appearance, especially in the stratified bowl. In a photo of an onion-slice experiment, regions where there has been a radial or vertical gradient of the zonal velocity show up with dye lines normal to that gradient. The more shear there has been, the more closely spaced these lines are.

Figure 12 shows onion-slice photos from a spin-up experiment in the stratified

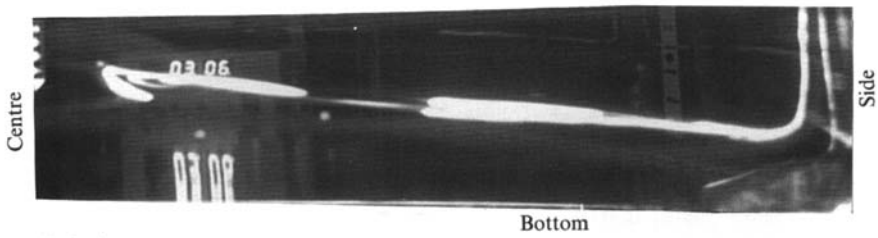

(*a*) 3 min

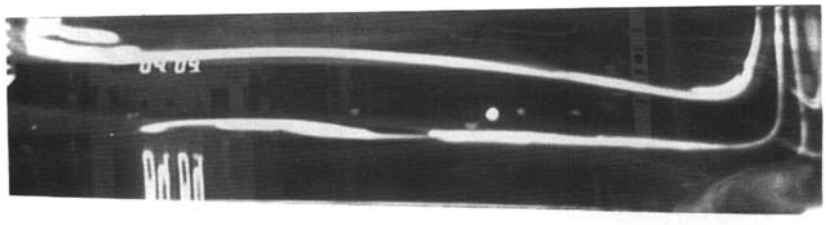

(*b*) 4 min

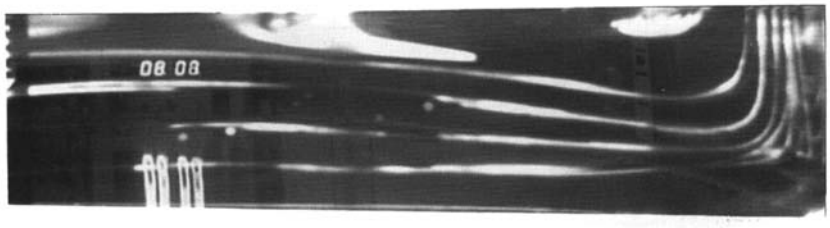

(*c*) 8 min

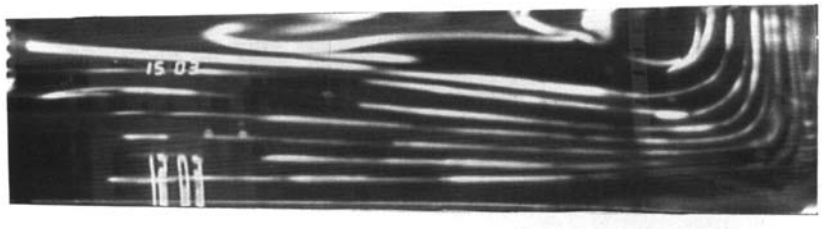

(*d*) 15 min

FIGURE 12. Onion-slice photos of a stratified spin-up experiment in the cylinder at four times, as listed. The container was spun-up 15% from $f = 1\ \mathrm{s}^{-1}$, and had a stratification similar to that shown in figure 6. The horizontal dye sheets bulged upward in the centre owing to the broadly distributed vertical shear of the zonal flow during 'fast' spin-up, while the sidewall boundary layer formed vertical sheets.

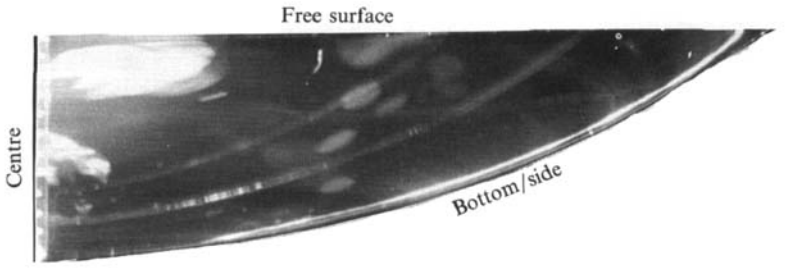

(*a*) 1.5 min

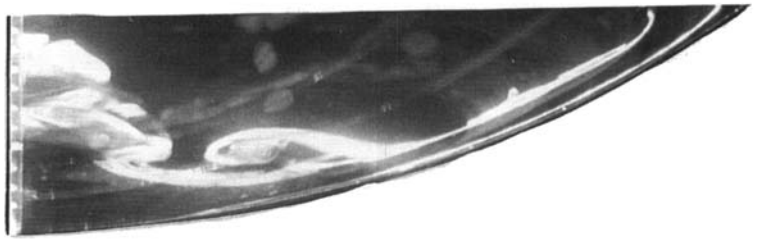

(*b*) 2.5 min

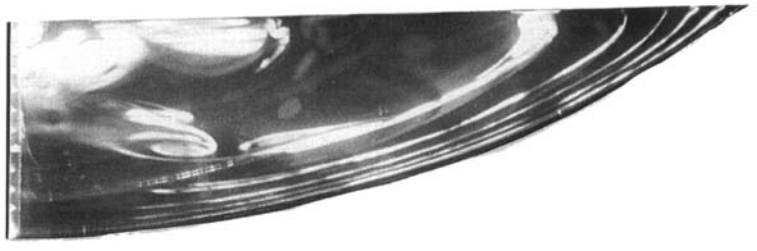

(*c*) 7 min

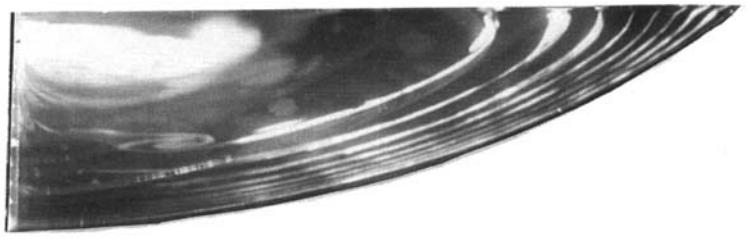

(*d*) 13 min

FIGURE 13. Same as figure 12, except in the bowl. Note that in (*a*) there was only one actual dye line, which lay close to the edge of bowl; the fainter lines were reflections. The adjusting flow was dominated by diffusive penetration normal to the boundary.

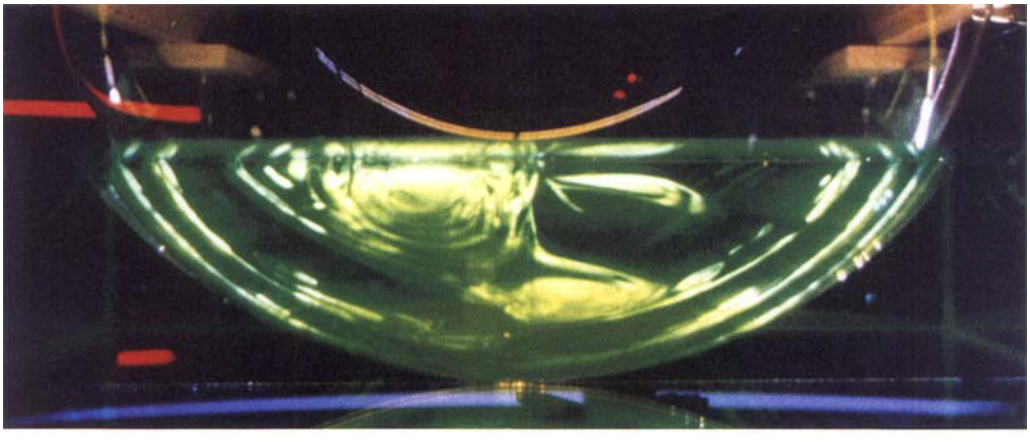

(*a*)

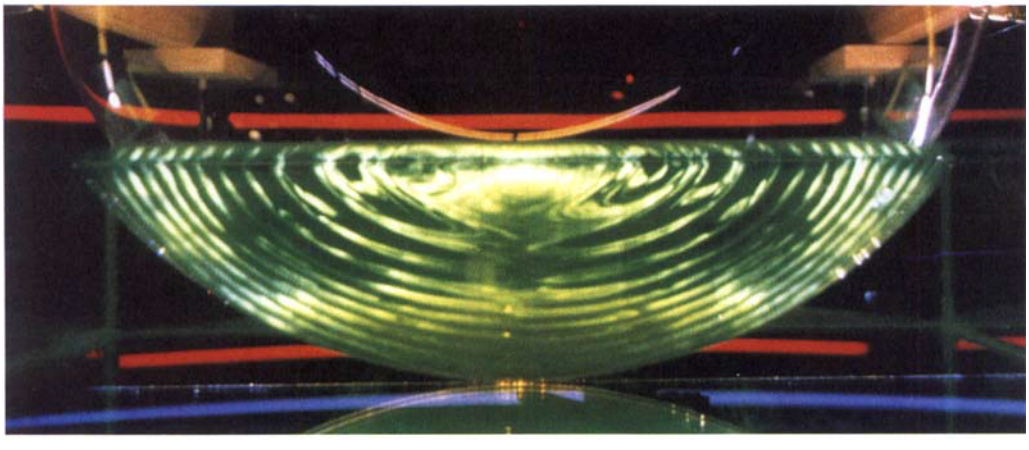

(*b*)

FIGURE 14. Colour photos of a stratified spin-up experiment in a hemispherical container, showing the complete fluorescein signal, (*a*) early in the experiment, and (*b*) at a later time. In general, the dye injected was initially rather messy, but the shear in the zonal velocity field sharpened the gradients of the dye, leading eventually to well-defined lines in the light sheet.

cylinder, and figure 13 shows photos from an experiment in the stratified bowl, graphically demonstrating the different nature of the flow in the two containers. In the first two photos of the cylinder (figure 12*a*, *b*) the widely spaced dye lines nearly filled the body of the fluid, expressing the penetration of the 'fast' spin-up throughout most of the tank. Later (figure 12*d*) the shear had continued fairly evenly through the depth of the fluid. The dye surfaces bowed upwards from the bottom centre where 'fast' spin-up was most intense, while a zonal differential jet near the outer wall represented fluid that was only slowly spun-up. The diffusive inward penetration near the outer wall was reflected in the vertical strike of the dye lines there. Fluid which had been transported radially outward in the bottom Ekman layer could be seen as a wedge in the corner of the cylinder. This wedge was the finite-Rossby-number expression of the circumferential forcing of the interior by the boundary layer flow.

Experiments in the bowl, figure 13 and figure 14 (plate 1), showed remarkably smooth quasi-diffusion of momentum inward from the sloping bottom. Early in an experiment, figure 13(*a*), just a single dye sheet was visible near the boundary. The inner core of fluid had made about one revolution relative to the boundary. At this rotation rate ($f = 1\ \mathrm{s}^{-1}$), intermediate between the two cases shown in figures 9 and 10, there was little sign of significant 'fast' classical spin-up, which would cause an upward bowing of the deeper dye sheets. Regions free of dye lines represent unsheared fluid, rotating at nearly their original angular velocity. In this core there was a slight 'fast' spin-up even in the cases with rapidly shut-down boundary layers (e.g. the inner core of figure 9(*b*) experiences weak spin-up without waiting for diffusion from the boundary).

Looking at spin-up in a variety of containers we found a consistent tendency for the dye sheets to mimic the shape of the lower boundary. Figure 12 represents perhaps the most extreme violation of this result, in the case of an extensive horizontal bottom above which the Ekman layer can continue to flow.

6. Comparison of theory with laboratory experiments

The theoretical ideas of shut-down and slow diffusion developed in §2 may be useful in understanding the experimental results if we assume that the experimental boundary layer developed in accordance with its *local* flow parameters. This approximation is commonly made for geophysical boundary layers when the scale of variation of the relevant parameters, such as N and V, is much greater than the boundary-layer thickness. Since N and V typically vary in our experiments only over the depth and radius of the bowl, we expect our local theory to be valid until the boundary layer has 'slow diffused' a good portion of the depth into the fluid. If significant fast spin-up has occurred then we would have to take account of the space–time structure of V in applying the theory.

Figure 15 shows the shut-down time τ versus radius, for the two bowl experiments. In the small-f experiment there was almost no sign of fast spin-up, particularly for the shallow beads. The brevity of the shut-down time implied that there would be essentially no radial boundary-layer transport, and hence no fast spin-up outside $r = 10$ cm. Fast spin-up inside that radius would penetrate less than one-third of the full depth at the centre, barely affecting the deeper beads. Thus the small-f swirl velocity data appear consistent with the interpretation that the boundary-layer transport was strongly limited by the shut-down mechanism.

In the large-f experiment there was evidence of some 'fast' spin-up, although not

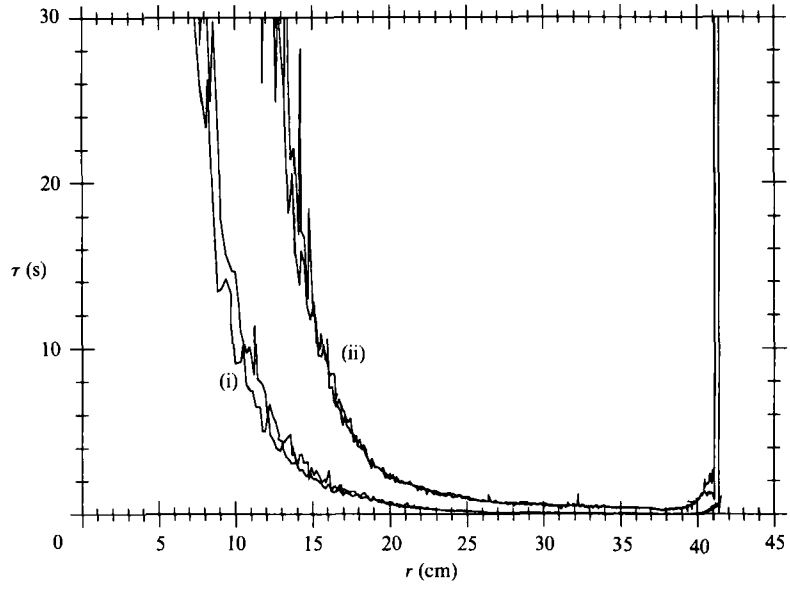

FIGURE 15. Shut-down time at the lower boundary versus radius for two bowl spin-up experiments: (i) refers to the experiment whose velocity data are shown in figure 9 (small-f), and (ii) refers to the experiment whose velocity data are shown in figure 10 (large-f). There are two profiles for each experiment since an experiment had to be performed twice in order to measure velocity at the two different depths.

nearly as much as in the cylinder, nor for as long. In the cylinder 'fast' spin-up occurred for about 3 min, whereas in the bowl with large-f it only lasted about 1 min. The shut-down time implied little transport outside of $r = 15$ cm. Owing to the increased rotation rate, the e-folding height of the region of fast spin-up would extend through about two-thirds of the depth of the fluid, affecting both deep and shallow beads. The large-f data are thus also qualitatively consistent with the shut-down hypothesis.

Assuming that the small-f experiment was, over most of its radius, unaffected by 'fast' spin-up, we may compare the angular velocity with that predicted by the slow-diffusion equation. Figure 16 shows angular velocity versus time at four locations in the small-f experiment. Also shown are predicted slow-diffusion solutions based on the value of $\nu S/(1+S)$ at the boundary nearest to the position in question. The three comparisons at larger radius are fairly close, indicating that slow diffusion was probably a good description of the situation. An alternative hypothesis is that the time rate-of-change of the zonal velocity was due to meridional circulation driven by whatever boundary-layer transport was present, and not slow diffusion. Without knowing the actual boundary-layer transport it is difficult to prove or disprove this idea, and we may say only that the data are consistent with slow diffusion. The innermost comparison (figure 16*d*) diverged strongly from the slow-diffusion prediction. This was probably due to the effects of 'fast' spin-up near the centre. Similar data for the large-f experiment (not shown here) also diverged strongly from the slow-diffusion prediction, again presumably due to the effects of 'fast' spin-up.

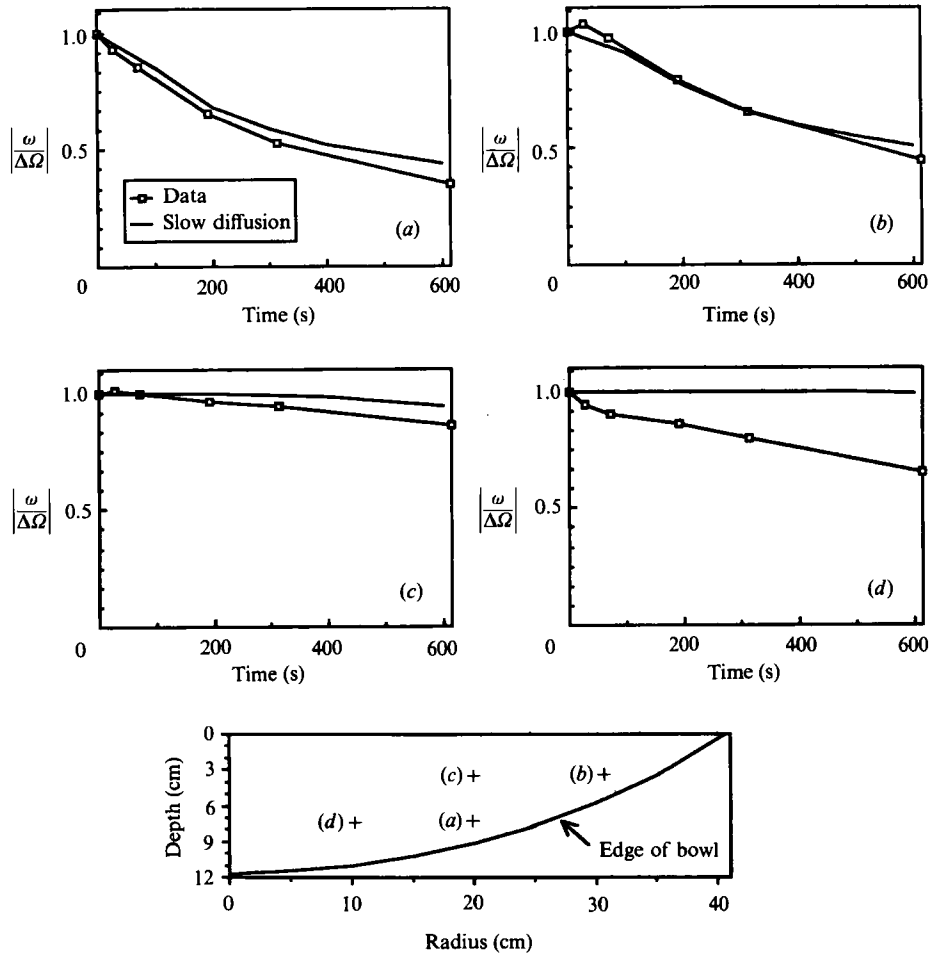

FIGURE 16. Normalized angular velocity versus time, at four different locations during the small-f (refer to figure 9) stratified spin-up experiment in the bowl, compared with velocities predicted by local solutions to the slow diffusion equation (2.20). The four locations are shown schematically at the bottom.

7. Conclusion

Our analysis of the boundary layer for rotating, stratified flow along a slope led to a circulation markedly different from that of an Ekman layer. It was neither steady, nor was it simply related to the interior velocity. Instead, the velocity profiles, and the cross-slope transport, were in general highly time-dependent. Buoyancy forces due to advection and diffusion of the stratification modified the force balance, tending to resist up- or down-slope velocities.

Very soon after its initiation the flow began to resemble an Ekman layer, but at large t/τ the flow looked like the steady solution (2.13) of Thorpe (1987), which allows only one interior along-slope velocity, and only one cross-slope transport. These properties make Thorpe's solution difficult to apply to geophysical situations. Thorpe (1987) and Garrett (1990) addressed this difficulty by modifying the steady theory to include depth-varying profiles of viscosity and diffusivity, which could be interpreted as saying that a given internal geostrophic flow exerts control over the

magnitude of turbulent diffusion near the boundary. We have taken a different approach, trying to make the boundary-layer representation more realistic by allowing time dependence. In doing so we found that there was a whole continuum of solutions between those of Ekman and Thorpe.

The 'slow diffusion' equation (2.20) predicted that the boundary condition on the along-slope velocity would diffuse into the interior, and the numerical simulations of §3 implied that the eventual boundary condition for this equation was the interior velocity of Thorpe's solution (which vanishes as $\kappa \to 0$). What is of interest about slow diffusion is that it actually penetrates the interior much like a non-rotating viscous boundary layer, in contrast to both Ekman and Thorpe's solutions which remain confined close to the boundary.

In §2 we also predicted the temporal evolution of the cross-slope transport. With the aid of numerical solutions to determine an unknown constant, we found that the transport changed smoothly from the initial Ekman-layer value to the final value of Thorpe's solution over a timescale τ (2.28), the 'shut-down time'.

The shut-down time gives a sensible way to evaluate what sort of boundary-layer theory we should be using for a given situation. If the flow is varying much more rapidly than the shut-down time, say owing to the effects of 'fast' spin-up, then standard Ekman theory is a good approximation. If we are only interested in the flow long after the shut-down time, and only over a region where slow diffusion will have accomplished its work without being countermanded by other circulations or buoyancy sources, then Thorpe's steady solution is appropriate. Yet anywhere between these two limits we must necessarily be aware of the unsteady nature of the boundary layer.

The stratified spin-up experiments in a bowl with a sloping bottom boundary described in §4 and 5 occupy a regime where slow diffusion and the shut-down time were very important. Over much of the bowl with small-f the shut-down time was so short that almost no up-slope transport was allowed, and hence almost no 'fast' spin-up occurred. In these cases the main decrease in zonal velocity was apparently due to slow diffusion. In the bowl spin-up experiments the large-scale dynamics were completely altered by the buoyancy modification of the boundary layer. Although the bowl was everywhere shallower than a cylinder wherein comparison experiments were done, the fluid in the bowl spun-up much more slowly than that in the cylinder. Thus, by varying the geometry of the experiment we ended up with a boundary that effectively had significantly lower drag than that of the cylinder.

If the interior circulation is naturally oscillatory (as, for example, with a Rossby wave), these boundary-layer dynamics imply a frequency-dependent 'bottom friction' which is strong only at high frequencies, where the flow changes direction before shut-down can occur.

We may make a simple estimate of the along-slope stress that the boundary exerts upon the fluid using the equations developed in §2. Taking $\hat{z}$-integrals of the rotated equations of motion (2.7) with boundary conditions (2.8) and solving for the boundary stress in terms of the integrated cross-slope transport M (again with vanishingly small R_t and E_s) we find

$$-\nu\rho_0 \frac{\partial \hat{v}}{\partial \hat{z}} = \rho_0 f \cos\alpha \,[M(1+S) - S\kappa \cot\alpha] \quad \text{at} \quad \hat{z} = 0, \tag{7.1}$$

or

$$-\nu\rho_0 \frac{\partial \hat{v}}{\partial \hat{z}} \approx M\rho_0 f \cos\alpha \quad \text{at} \quad \hat{z} = 0 \quad \text{for} \quad S \ll 1. \tag{7.2}$$

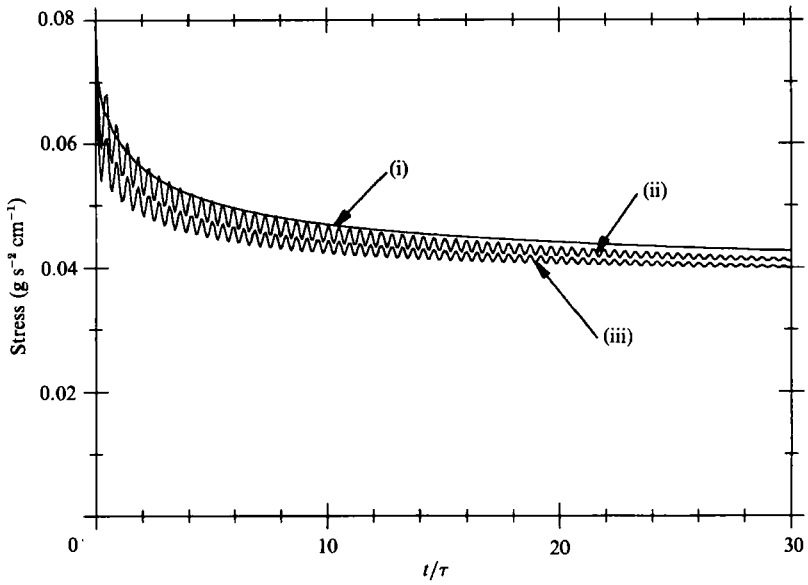

FIGURE 17. Along-slope stress at $\hat{z} = 0$ from a numerical solution to (2.7) with all parameters as in figure 3(*a*). The actual stress, $-\nu\rho_0(\partial\hat{v}/\partial\hat{z})$, is shown by curve (i), while curve (ii) shows the stress estimated from the right-hand side of (7.1), and curve (iii) shows the stress estimated from the right-hand side of (7.2).

The last expression (7.2) is exact for both the Ekman layer and Thorpe's solution, simply expressing that the boundary stress is balanced by the Coriolis force on the cross-slope transport. For the time-dependent boundary layer the boundary stress is balanced both by the Coriolis force and the acceleration of the along-slope flow. Equation (7.2) tells us that, for S small (which we expect for small slopes), the acceleration term is negligible and the stress is tied to the transport, exactly as in the steady theories. One may question the validity of (7.2) on the grounds that it is an estimate of stress in a region where E_s is likely to be large, violating our assumptions. Yet since we are using $\hat{z}$-integrals of the equations it turns out that the scale estimate of the $\hat{z}$-integrated viscous term in (2.7*a*), divided by the $\hat{z}$-integrated Coriolis term, is $(U/V)(E_s^{\frac{1}{2}})(\delta_s/D_v)$. While the first two parts of this scale estimate may be $O(1)$ when $\sigma = 1$, the third term becomes small as the along-slope boundary layer 'slow-diffuses' into the interior. Figure 17 shows the along-slope stress at $\hat{z} = 0$ versus t/τ for a numerical run with $\sigma = 1$ and $S = 0.29$ (all parameters as in figure 3*a*). We also plot the right-hand sides of (7.1) and (7.2). The figure demonstrates that, even in a case with strong density diffusion and S not far from 1, the boundary stress is approximately equal to the Coriolis force on the cross-slope transport. This balance is ironic when we consider that the slow-diffusion equation implies that boundary stress balances along-slope acceleration when $\sigma = 1$. But from the numerical simulations (§3) we know that the slow-diffusion equation gives a poor representation of boundary stress when $\sigma = 1$. As $\sigma \to \infty$ the slow-diffusion solution was nearly perfect at the boundary and indeed, in this case its $\hat{z}$-integral is exactly equal to (7.1). For the stratified spin-up experiments (7.1) shows that the torque exerted by the bowl upon the fluid dropped off rapidly as the up-slope transport was shut-down by buoyancy forces.

The boundary-layer theory developed in §2 is only applicable if the assumptions that went into its development are reasonably satisfied. We assumed constant

viscosity, diffusivity, and stratification, we ignored variations along or across the slope, and we ignored the overturning of statically unstable stratifications. To make the theory more geophysically relevant the most important direction to pursue would be the inclusion of variable viscosity and diffusivity, as Thorpe (1987) and Garrett (1990) have done for the steady theory. We hope to pursue this avenue in future work.

In the atmosphere, the low thermal mass of air, combined with radiative means of changing temperature, make a conducting boundary condition on the density realistic. This boundary condition allows relatively simple Ekman-like boundary-layer solutions (Holton 1967 and Hsueh 1969). In contrast, the ocean floor is best modelled as an insulating boundary, except in the few areas of geothermal heating. Hence it is in the ocean that we expect our theory could be used. There are practical difficulties, though, with applying any theory of the oceanic bottom boundary layer. Data are very scarce, and determining turbulent coefficients of viscosity and diffusivity is inexact. It is generally accepted that in a turbulent mixed layer near the boundary the Prandtl number may be close to one. Yet stratified turbulence may easily send its energy into internal wave motion, which can transport momentum far from the boundary, leading to either a very high Prandtl number or the abandonment of Fickian diffusion entirely.

As a lowest-level approximation, let us assume that the ocean has a constant vertical eddy diffusivity, K, given by Munk's (1966) canonical value of 1 cm^2 s^{-1}. Thorpe's steady transport, $K\cot\alpha$, is then simply a function of the bottom slope. Note that the transport becomes infinite as the slope goes to zero, and so is certainly unphysical over flat areas (the interior along-slope velocity also goes to infinity in this case). Consider two regions in the ocean: a continental slope with relatively strong stratification, and an abyssal region with less slope and a small stratification. Over the sloping region, with $\tan\alpha = 10^{-2}$ and $N = 3.5\times10^{-3}$ s^{-1}, Thorpe's transport becomes very small, having up-slope velocities of only 0.1 cm s^{-1} if distributed over a 10 m thickness. The shut-down time indicates that the transport begins to approach this small value in about a week. Over an abyssal plane, with $\tan\alpha = 10^{-3}$ and $N = 10^{-3}$ s^{-1}, Thorpe's transport is large enough to be important, 1 cm s^{-1} if distributed over a 10 m thickness. Yet this value is only achieved over the shut-down time, which is 3×10^4 years. These are only rough estimates, which do not account for variable viscosity and diffusivity. They do indicate, however, that shut-down may be very important on continental slopes, while standard Ekman theory is useful over an abyssal plane. A yardstick to judge the possible importance of shut-down is that the e-folding timescale of ocean currents due to 'fast' spin-up is typically taken as one year in numerical models. Any shut-down time shorter than this is likely to influence the evolution of flow along the ocean's bottom boundary.

In general, the shut-down time and its supporting theory presented in §2 should help in determining when and how buoyancy becomes important to the boundary-layer force balance in a given situation.

This work was supported by National Science Foundation grant no. 8613725, and Office of Naval Research grant no. N00014-86-K-0690. The authors wish to thank Chris Garrett for his continued interest in this work, and in particular for his helpful insight about the slow-diffusion equation. We also wish to thank Trevor McDougall, Angus McEwan, the laboratory group at CSIRO, Hobart, Tasmania, as well as Eric Semtner. Portions of this work were previously reported at the 'Aha Huliko'a Hawaii Winter Workshop, 1989, and at the American Geophysical Union Fall 1989 Meeting.

REFERENCES

BENTON, E. R. & CLARK, A. 1974 Spin-up. *Ann. Rev. Fluid Mech.* **6**, 257–280.

BUZYNA, G. & VERONIS, G. 1971 Spin-up of a stratified fluid: theory and experiment. *J. Fluid Mech.* **50**, 579–608.

GARRETT, C. 1982 On spindown in the ocean interior. *J. Phys. Oceanogr.* **12**, 989–993.

GARRETT, C. 1990 The role of secondary circulation in boundary mixing. *J. Geophys. Res.* **95**, 3181–3188.

GILL, A. E. 1981 Homogeneous intrusions in a rotating stratified fluid. *J. Fluid Mech.* **103**, 275–295.

GREENSPAN, H. P. & HOWARD, L. N. 1963 On a time-dependent motion of a rotating fluid. *J. Fluid Mech.* **17**, 385–404.

HOLTON, J. R. 1965 The influence of viscous boundary layers on transient motions in a stratified rotating fluid: Part I. *J. Atmos. Sci.* **22**, 402–411.

HOLTON, J. R. 1967 The diurnal boundary layer wind oscillation above sloping terrain. *Tellus* **19**, 199–205.

HSUEH, Y. 1969 Buoyant Ekman layer. *Phys. Fluids.* **12**, 1757–1762.

MUNK, W. H. 1966 Abyssal recipes. *Deep-Sea Res.* **13**, 707–730.

PEDLOSKY, J. 1987 *Geophysical Fluid Dynamics.* Springer.

PHILLIPS, O. M. 1970 On flows induced by diffusion in a stably stratified fluid. *Deep-Sea Res.* **17**, 435–443.

PHILLIPS, O. M., SHYU, J.-H. & SALMUN, H. 1986 An experiment on boundary mixing: mean circulation and transport rates. *J. Fluid Mech.* **173**, 473–499.

SIEGMANN, W. L. 1971 The spin-down of rotating stratified fluids. *J. Fluid Mech.* **47**, 689–711.

ST-MAURICE, J.-P. & VERONIS, G. 1975 A multi-scaling analysis of the spin-up problem. *J. Fluid Mech.* **68**, 417–445.

THORPE, S. A. 1987 Current and temperature variability on the continental slope. *Phil. Trans. R. Soc. Lond.* A **323**, 471–517.

WALIN, G. 1969 Some aspects of time-dependent motion of a stratified rotating fluid. *J. Fluid Mech.* **36**, 289–307.

WEATHERLY, G. L. & MARTIN, P. J. 1978 On the structure and dynamics of the oceanic bottom boundary layer. *J. Phys. Oceanogr.* **8**, 557–570.